

1 **A New WRF-Chem Treatment for Studying Regional**
2 **Scale Impacts of Cloud Processes on Aerosol and Trace**
3 **Gases in Parameterized Cumuli.**

4
5 **L. K. Berg¹, M. Shrivastava¹, R. C. Easter¹, J. D. Fast¹, E. G. Chapman¹, Y.**
6 **Liu¹, and R. A. Ferrare²**

7 [1] Pacific Northwest National Laboratory, Richland, WA, USA

8 [2] NASA Langley Research Center, Hampton, VA, USA

9 Correspondence to: L. K. Berg (larry.berg@pnnl.gov)

10 **Abstract**

11 A new treatment of cloud effects on aerosol and trace gases within parameterized shallow
12 and deep convection, and aerosol effects on cloud droplet number, has been implemented
13 in WRF-Chem that can be used to better understand the aerosol lifecycle over regional to
14 synoptic scales. The modifications to the model include treatment of the cloud droplet
15 number mixing ratio; key cloud microphysical and macrophysical parameters (including
16 the updraft fractional area, updraft and downdraft mass fluxes, and entrainment) averaged
17 over the population of shallow clouds, or a single deep convective cloud; and vertical
18 transport, activation/resuspension, aqueous chemistry, and wet removal of aerosol and
19 trace gases in warm clouds. These changes have been implemented in both the WRF-
20 Chem chemistry packages as well as the Kain-Fritsch cumulus parameterization that has
21 been modified to better represent shallow convective clouds. Testing of the modified
22 WRF-Chem has been completed using observations from the Cumulus Humilis Aerosol
23 Processing Study (CHAPS) as well as a high-resolution simulation that does not include
24 parameterized convection. The simulation results are used to investigate the impact of
25 cloud-aerosol interactions on regional scale transport of black carbon (BC), organic
26 aerosol (OA), and sulfate aerosol. Based on the simulations presented here, changes in
27 the column integrated BC can be as large as -50% when cloud-aerosol interactions are
28 considered (due largely to wet removal), or as large as +40% for sulfate in non-

1 precipitating conditions due to sulfate production in the parameterized clouds. The
2 modifications to WRF-Chem version 3.2.1 are found to account for changes in the cloud
3 drop number concentration (CDNC) and changes in the chemical composition of cloud-
4 drop residuals in a way that is consistent with observations collected during CHAPS.
5 Efforts are currently underway to port the changes described here to the latest version of
6 WRF-Chem, and it is anticipated that they will be included in a future public release of
7 WRF-Chem.

8

9 **1 Introduction/motivation**

10 There remains a significant amount of uncertainty related to both the aerosol direct
11 forcing and aerosol indirect effects (e.g. Solomon et al., 2007; Boucher et al., 2013).
12 Numerical models of the atmosphere are one of the common tools used to investigate
13 these effects. High-resolution simulations using horizontal grid spacing less than 10 km,
14 which can explicitly represent convective clouds and cloud-aerosol interactions, have
15 been widely used for short-term studies of cloud-aerosol interactions (e.g. Qian et al.,
16 2009; Wang et al., 2011; Fan et al., 2012). They have not, however, generally been used
17 for long-term simulations because of the associated computational expense. For long-
18 term simulations, coarser horizontal resolution is generally required that necessitates the
19 use of a cumulus parameterization even if the cloud-aerosol interactions associated with
20 sub-grid scale convective clouds are poorly represented (e.g. Zhao et al., 2011). Thus,
21 treatments of aerosols in cumulus parameterizations are needed for investigations of the
22 impact of clouds on aerosol mixing, transformation, and removal as well as the impact of
23 aerosol on cloud properties (Stevens and Feingold, 2009).

24 Shrivastava et al. (2013) compared changes in the aerosol chemical composition and
25 cloud microphysical structure associated with cloud-aerosol interactions in fields of
26 shallow cumuli to data collected during the Cumulus Humilis Aerosol Processing Study
27 (CHAPS; Berg et al., 2009). The main goal of CHAPS was to find evidence of cloud-
28 aerosol interactions in fields of shallow cumuli. The simulations presented by Shrivastava
29 et al. (2013) were completed with sufficiently high resolution that a convective
30 parameterization was not required allowing them to investigate cloud-aerosol interactions

1 in relatively small shallow clouds that would be sub-grid scale at coarser resolutions.
2 Among their findings were systematic changes in the chemistry of activated particles and
3 cloud microphysics within shallow cumuli. They found that nitric acid vapor uptake by
4 cloud droplets led to increased nitrate content in the cloud droplet residuals. They also
5 reported changes in cloud microphysical properties, with increases in cloud droplet
6 number concentration and decreases in droplet effective radius with an increase in
7 pollutant loading.

8 The Weather Research and Forecasting model coupled with Chemistry (WRF-Chem)
9 (Grell et al., 2005; Fast et al., 2006) is frequently used to simulate conditions over a range
10 of spatial scales and has been used to study a wide range of atmospheric phenomena
11 associated with atmospheric chemistry and aerosols (e.g. McKeen et al., 2007; Ntelekos
12 et al., 2009; Grell et al., 2011; Pfister et al., 2011; Ahmadov et al., 2012; Matsui et al.,
13 2013). To date, however, the treatment of cloud-aerosol interactions has largely been
14 limited to grid-resolved clouds (Chapman et al., 2009). This is the case for WRF coupled
15 with the Community Atmospheric Model version 5 (CAM5; Neale et al., 2012) physics
16 parameterizations, although cloud-aerosol interactions in convectively detrained
17 stratiform clouds are treated (Ma et al., 2013). One exception is the recent modification
18 of the Grell cumulus parameterization (Grell, 1993; Grell and Dévényi, 2002) to include
19 aqueous chemistry using Community Multiscale Air Quality (CMAQ) routines and
20 aerosol interactions in the conversion of cloud water to rainwater and the evaporation of
21 rain (Grell and Freitas, 2013). Lim et al. (2013) added a treatment of aerosol activation to
22 the Zhang-McFarlane parameterization (Zhang and McFarlane, 1995) while Zhao et al.
23 (2013) modified the Kain Fritsch scheme to better account for transport and wet
24 scavenging of dust, but each of their modifications do not include treatment of aqueous
25 chemistry in the clouds nor have they been added to the publicly released version of
26 WRF-Chem. To address this missing process, we have modified WRF-Chem to include
27 treatments of a number of factors and processes important for accurately representing
28 aerosol and trace gases within sub-grid convective clouds, including: fractional coverage
29 of active and passive clouds, vertical transport, activation and resuspension, wet removal,
30 and aqueous chemistry for cloud-borne particles. The new parameterization uses the
31 Model for Simulating Aerosol Interactions and Chemistry (MOSAIC; Zaveri et al., 2008)

1 packages to represent the aerosol chemistry. This new treatment is important to include
2 additional realism in regional scale modeling studies that require the use of cumulus
3 parameterizations when investigating the effects of clouds on aerosol and the effects of
4 aerosol on clouds. It should be noted, however, that the modifications do not yet include
5 feedbacks of aerosol on the amount of precipitation, or feedbacks between the cumulus
6 microphysics and the radiation. These additions are topics for subsequent research.

7 The work presented here describes the implementation of a treatment of activation,
8 vertical transport, aqueous chemistry, and wet removal for sub-grid parameterized
9 convective clouds in WRF-Chem. Section 2.0 describes changes to both the standard
10 cumulus parameterization and the treatment of processes affecting aerosol and trace gases
11 in the sub-grid convective clouds. These changes include improved treatment of cloud
12 fraction as well as treatment of cloud droplet number concentration, vertical transport,
13 activation/resuspension, aqueous phase chemistry, and wet removal. Section 3 provides a
14 description of the WRF-Chem configuration, simulation design, and emissions data used
15 in the study. The data used from CHAPS are presented in Section 4. Analysis of the
16 WRF-Chem simulations are presented in Section 5. Rather than focusing on only the
17 CHAPS study area, results are also presented from three different locations that were
18 selected to highlight the performance of the model in situations with shallow and deep
19 sub-grid convective clouds; and to document the impact on the regional scale transport,
20 cloud microphysics, and the chemical composition of cloud droplets.

21 **2 Modifications to WRF-Chem**

22 The primary goal of this effort has been to improve the representation of vertical
23 transport, aqueous chemistry, wet removal, and aerosol effects on cloud droplet number
24 in parameterized sub-grid convective clouds within WRF-Chem. To address this goal, a
25 number of modifications shown schematically in Figure 1, have been made to WRF-
26 Chem in order to account for cloud-aerosol interactions within these clouds. These
27 modifications include changes to the Kain-Fritsch (KF) cumulus scheme (Kain and
28 Fritsch, 1990; Kain, 2004) as well as changes designed to account for transport,
29 transformation, and removal of aerosols and trace gases within sub-grid convective
30 clouds.

1 The WRF-Chem model architecture separates physical processes involving sub-grid
2 cumulus, microphysics for grid-resolved clouds, boundary-layer turbulence, and radiation
3 from processes involving aerosol and trace gases. We have followed this separation, so
4 that code changes involve both a cumulus physics routine that determines the presence of
5 sub-grid convective clouds, their properties, and their impacts on heat, moisture, and
6 momentum, and a separate cumulus aerosol and trace gas routine that treats vertical
7 transport, activation/resuspension, aqueous chemistry, and wet removal of aerosol and
8 trace gases. Modifications to the cumulus physics routine are described in sections 2.1.1,
9 2.1.2, and 2.2.1. The cumulus aerosol and trace gas routine, which is new to WRF-Chem,
10 is described in section 2.2.2.

11 **2.1 Modifications to the Kain-Fritsch cumulus parameterization**

12 **2.1.1 Trigger function for convection**

13 Recently, the KF scheme has been modified to improve the treatment of shallow cumuli,
14 which are defined by the KF scheme to be less than 2 to 4 km in height, depending on the
15 temperature at the lifting condensation level. These changes were made primarily within
16 the standard KF (Kain and Fritsch, 1990; Kain, 2004) convective parameterization and
17 involved replacing the default ad-hoc trigger function used in the parameterization with
18 one explicitly linked to the boundary-layer turbulence. This was accomplished using the
19 Cumulus Potential (CuP) scheme (Berg and Stull, 2005) leading to the new KF-CuP
20 parameterization (Berg et al., 2013). These changes were designed to better account for
21 sub-grid variability by applying a range of temperature and moisture perturbations from
22 the grid-box mean as the convective trigger, thus allowing a population of shallow clouds
23 with different thermodynamic properties to coexist in a model grid column. In the case of
24 deep convection, only the single most probable temperature and moisture perturbation
25 that triggered clouds is applied to be consistent with the standard implementation of the
26 KF scheme. The sub-grid distribution of temperature and humidity was parameterized
27 using probability density functions (PDFs) of temperature and humidity that were based
28 on the jump of potential temperature and moisture at the surface and at the boundary-
29 layer top (Berg and Stull, 2004). These modifications, along with the cloud fraction
30 changes (Section 2.1.2), were shown to significantly increase the frequency of occurrence

1 of simulated shallow clouds over the Southern Great Plains, leading to improved
2 forecasts of both cloud fraction and downwelling shortwave irradiance (Berg et al.,
3 2013). It should also be noted that while the new trigger function is not scale aware, it
4 could easily be modified to adjust the PDF based on the model grid spacing.

5 **2.1.2 Cloud fractional area**

6 In their modifications to the standard KF scheme, Berg et al. (2013) included a simple
7 treatment of the cloud fraction associated with sub-grid scale convective clouds. Their
8 method was based on representative time scales associated with cumulus, which the
9 method defined to be a function of the cloud depth, turbulence intensity, and the moisture
10 in the cloudy layer. In the work presented here, an additional treatment was added to
11 determine the cloud fractional area for instances with deep convection. Rather than
12 develop a new representation of the total cloud fraction for deep convection the empirical
13 treatment used in CAM5 is applied. In this parameterization the cloud fraction associated
14 with deep convection is a function of the convective mass flux (Neale et al., 2012), and is
15 represented as:

$$16 \quad \sigma_{dp,cu} = k_{1,dp} \ln(1 + k_2 M_{dp,cu}), \quad (1)$$

17 where $\sigma_{dp,cu}$ is the cloud fraction associated with deep-convective clouds, $k_{1,dp}$ is an
18 adjustable parameter set to 0.1, k_2 is assumed to be 675, and $M_{dp,cu}$ is the updraft mass
19 flux of the convective clouds (in $\text{kg m}^{-2} \text{s}^{-1}$). The values of both $k_{1,dp}$ and k_2 were selected
20 to be the same as the values used in CAM5, and are identical to those used by Ma et al.
21 (2013) in their implementation of the CAM5 physics in WRF and made publically
22 available in version 3.5 and are similar to that proposed by Alapaty et al. (2012) and
23 Herwehe et al. (2014). It could be argued that a parameterization of cloud fraction
24 developed for a relatively coarse resolution model like CAM5 is not appropriate for a
25 regional scale model like WRF, which can be run at a wide range of resolutions. When
26 run at high horizontal resolution, however, the cumulus parameterization is generally
27 turned off so that the parameterization of sub-grid convective cloud fraction is not
28 utilized. Given the constants define above, (1) predicts the maximum cloud fraction in the
29 grid cell associated with deep convection to be approximately 45%. Similar to the

1 methodology applied by Berg et al. (2013) for cases of shallow cumuli, the deep-cloud
2 fraction computed using (1) is applied in the radiation parameterization but has no impact
3 on either the convective tendencies for heat, moisture, momentum or on the cumulus
4 transport of aerosols and trace gases. It is, however, used in the computations related to
5 aqueous chemistry described in Section 2.2.

6 The cloud fraction associated with both shallow and deep sub-grid convective clouds is
7 broken further into two sub-types: active and passive clouds (e.g. Stull, 1985). Active
8 clouds are those that have vigorous updrafts and contribute to the upward cloud mass
9 fluxes. The fractional area of active cumulus for shallow clouds is defined as the fraction
10 of the PDF of temperature and humidity applied in the convective scheme that forms
11 clouds, while for deep clouds it is the standard KF updraft fraction area. Passive clouds
12 consist primarily of decaying clouds without a well-organized updraft. The fractional area
13 of the passive clouds is determined as the difference between the total cloud fraction
14 [computed following Berg et al. (2013) for shallow clouds, and Eq. 1 for deep clouds]
15 and the active cloud fraction that is determined within the KF-CuP scheme. Passive
16 clouds are treated as quiescent and are assigned zero vertical velocity, so that there is no
17 vertical mass flux. They are assumed to have the same total cloud water and ice content
18 as the active clouds, but be non-precipitating, so there is no wet removal associated with
19 passive clouds. In addition, when convective cloud is triggered in a model grid column,
20 the cloud population is assumed to be in steady state over the cloud lifetime defined in
21 the cumulus parameterization (30 minutes for shallow clouds and 30 to 60 minutes for
22 deep clouds).

23 **2.2 Modifications to account for vertical transport, aqueous chemistry,** 24 **wet removal, and cloud droplet number**

25 Chapman et al. (2009) described a treatment of cloud-aerosol interactions for grid
26 resolved clouds within WRF-Chem. For cloudy grid cells, the standard version of WRF-
27 Chem treats both cloud borne (activated) and interstitial (nonactivated) particles as
28 separate transported species. A number of modifications to the standard WRF-Chem
29 version 3.2.1 have been implemented in this study to specifically address cloud-aerosol
30 interactions in sub-grid convective clouds. These modifications include calculations for:

- 1 • Cloud droplet number mixing ratio
- 2 • Cloud microphysical (conversion rates, and cloud water and cloud ice mixing
- 3 ratios) and cloud macrophysical properties (updraft fractional area, updraft and
- 4 downdraft mass fluxes, and entrainment) averaged over the population of shallow
- 5 convective clouds, or for the single deep convective cloud value, and
- 6 • Vertical transport, activation/resuspension, aqueous chemistry, and wet removal
- 7 of aerosols and trace gases.

8 WRF-Chem has several different aerosol and trace gas representations, which are referred
9 to as chemistry packages. Our changes for sub-grid convective clouds were implemented
10 with the MOSAIC (Zaveri et al., 2008) sectional aerosol model and the SAPRC-99
11 photochemical mechanism (Carter, 2010). Extension to other WRF-Chem chemistry
12 packages would be relatively straightforward, especially those packages for which
13 aqueous chemistry and aerosol activation modules (or interfaces) already exist.

14 **2.2.1 Aerosol effects on the cloud droplet number**

15 Within the default KF scheme, as well as other cumulus parameterizations applied in
16 WRF, a highly simplified treatment of cloud microphysics is used. Cloud water is
17 produced in updrafts and converted to precipitation based on a prescribed e-folding
18 height, and additional assumptions are made involving frozen condensate and
19 precipitation and detrainment to downdrafts (e.g. Kain and Fritsch, 1990). While such a
20 simplified treatment has been successful for mesoscale weather forecasting, it is not
21 sufficient for studying cloud-aerosol interactions that are intimately linked to the cloud
22 microphysics. Thus, the activation of cloud drops in convective drafts must be
23 considered. The activation is a function of the cloud updraft speed and the number, size,
24 and composition of particles. In the modified version of the KF parameterization in
25 WRF-Chem that accounts for the cloud droplet number, the updraft velocities associated
26 with the buoyancy excess are computed using the temperature and humidity perturbations
27 for the range of parcels identified by the KF-CuP parameterization that form clouds.
28 Further, the droplet activation for each perturbation is computed by applying an
29 entraining parcel conceptual model using the Abdul-Razzak and Ghan (2000)
30 parameterization modified to account for entrainment following Barahona and Nenes

1 (2007). Once the droplet number concentrations are computed for each perturbation value
2 of temperature and humidity in the PDF, they are averaged together to provide a single
3 value of cloud droplet number concentration for each grid cell. Above cloud base, the
4 number of cloud droplets is further reduced by entrainment, where the entrainment rates
5 are determined using the KF scheme (averaged over all of the parcel perturbations to
6 yield a single entrainment rate). At present, secondary activation is not considered for
7 either sub-grid convective clouds or for high-resolution (cloud-resolving) simulations of
8 cumulus convection. In addition, the activation does not feedback on the cumulus clouds
9 via changes in the conversion of cloud water to rain (as treated by Grell and Freitas,
10 2013).

11 **2.2.2 Effects of sub-grid cumulus on aerosol and trace gases**

12 A new module was introduced to WRF-Chem to calculate the effects of sub-grid
13 convective clouds on aerosol and trace gases, including vertical transport,
14 activation/resuspension, aqueous chemistry in cloud droplets, and wet removal. The new
15 module has separate sections that treat the active clouds (as well as vertical transport in
16 the subsiding environment surrounding the active clouds) and passive clouds (for which
17 the only process is aqueous chemistry).

18 In models of the cloud (and precipitation) effects on aerosols and trace gases, one must
19 consider the attachment state (Ghan and Easter, 2006) of (aerosol) particles and gases.
20 For example, interstitial aerosol particles (i.e., particles suspended in air) may become
21 attached to, dissolved in, or suspended in various hydrometeors (cloud and rain drops, ice
22 crystals, snow and graupel particles). When the aerosol representation involves several
23 size bins (8 in our study) and multiple chemical species within each bin (14 in our study),
24 the computational expense of explicitly treating all possible attachment states is
25 considerable, and simplifying assumptions are often used. For example, in Chapman et al.
26 (2009) the treatment of cloud-aerosol interactions focused on grid-resolved warm clouds.
27 Aerosol material (sulfate, nitrate, etc.) associated with cloud droplets (referred to as
28 cloud-borne) of grid-resolved clouds was treated explicitly as transported prognostic
29 species, while moderately soluble gases dissolved in cloud droplets were assumed to be
30 in equilibrium with the gas-phase and were treated diagnostically. Aerosol material and

1 gases that became associated with precipitation particles (rain, snow, graupel) and also
2 ice crystals were assumed to be quickly removed from the atmosphere and were not
3 treated explicitly. A similar but somewhat simpler approach is used in our treatment of
4 sub-grid cumulus effects. For all attachment states, the aerosol species associated with
5 cloud droplets in the sub-grid convective clouds are treated explicitly, but only within the
6 convective cloud routines. This approximation is reasonable because of the relatively
7 short life-time of the parameterized convective clouds (30-60 minutes) and the fact that
8 the parameterization is intended for use with model horizontal grid spacings of
9 approximately 10 km or more. When air is detrained from sub-grid convective clouds,
10 any detrained cloud-borne aerosol is added to the grid resolved interstitial aerosol in that
11 grid box where the aerosol can potentially interact with resolved clouds.

12 The cumulus physics routine determines if sub-grid convective cloud is present within a
13 model grid column and the physical properties of the cumulus clouds (shallow or deep;
14 life-time; updraft and downdraft mass fluxes, entrainment, and vertical velocity; mixing
15 ratios of cloud water, ice, and precipitation; and microphysical conversion of cloud water
16 to cloud ice and precipitation) that are used in the cumulus effects routine. Within the
17 KF-CuP scheme, when deep convection is diagnosed within a grid column, the deep
18 clouds are assumed identical, and there is a single vertical profile for updraft and
19 downdraft mass fluxes and each microphysical parameter. When shallow convection is
20 diagnosed, there is a population of shallow clouds with different profiles, and downdrafts
21 are not treated. In the cumulus-effects-on-aerosols routine, calculations are made using
22 the properties of an average (over the population) shallow cloud, rather than doing
23 calculations for each shallow cloud in the population. This methodology is applied to
24 limit the information that is passed between the various WRF-Chem modules, to reduce
25 computational burden, and to allow the same treatment for shallow and deep cumuli. The
26 changes in aerosol properties associated with aqueous chemistry and transport in the
27 shallow clouds are less sensitive to the details of the cumulus updrafts than is the cloud
28 droplet number concentration.

29 Active cloud calculations are performed first, followed by passive cloud calculations. The
30 treatment of active sub-grid cumulus effects on aerosols and gases is very similar to the
31 unified treatment described in the supplementary material of Wang et al. (2013). The

1 active-cloud updrafts and downdrafts are treated as steady-state entraining plumes. The
 2 updraft and downdraft mass fluxes obey

$$3 \quad \frac{\partial M_Y}{\partial z} = \frac{(E_Y - D_Y)}{\Delta z} \quad (2)$$

4 where the Y subscript is either U for updraft or D for downdraft, M_Y is the mass flux (kg
 5 $\text{m}^{-2} \text{s}^{-1}$) defined at vertical layer boundaries, and E_Y and D_Y are the entrainment and
 6 detrainment in a layer, and Δz is the layer thickness. The compensating mass flux in the
 7 environment, M_E , is equal to $-(M_U + M_D)$. The active-cloud calculations involve
 8 integrating conservation equations for grid-cell mean mixing ratios of aerosol and trace
 9 gas species over the lifetime of the cumulus cloud. A time sub-step is used such that the
 10 transport of air out of a layer (by M_E , E_U , and E_D) during the sub-step does not exceed the
 11 layer's air mass $\rho \Delta z$, where ρ is the air density.

12 For each time sub-step, steady-state vertical profiles of aerosol and trace gas species in
 13 the updraft and downdraft are first calculated. This is done by integrating steady-state
 14 continuity equations upwards (for updrafts) or downwards (for downdrafts). For aerosol
 15 species in the updraft, the continuity equation is

$$16 \quad \frac{\partial (M_U q_{X,U})}{\partial z} = \frac{(E_U q_{X,E} - D_U q_{X,U})}{\Delta z} + \rho A_U \left[(\dot{q}_{X,U})_{ACTI} + (\dot{q}_{X,U})_{WETR} + (\dot{q}_{X,U})_{AQCH} \right] \quad (3)$$

17 Here $q_{X,E}$ and $q_{X,U}$ are aerosol mixing ratios in the environment (E) and updraft (U),
 18 respectively, the X subscript is either AI for interstitial aerosol species or ACC for
 19 convective-cloud-borne (activated) aerosol species. The environment mixing ratios for
 20 interstitial aerosol are assumed equal to the grid-cell mean values, and are zero for
 21 convective-cloud-borne aerosol. A_U is the updraft fractional area and is equal to
 22 $(M_U/\rho w_U)$, where w_U is the updraft vertical velocity. The last three terms on the right
 23 hand side are the rates of change due to activation ($ACTI$), in-cloud wet removal ($WETR$),
 24 and aqueous-phase chemistry within cloud droplets ($AQCH$). For interstitial aerosol, only
 25 the activation term is non-zero.

26 Aerosol activation is calculated as described in section 2.2.1, but with the simplification
 27 of using the average (over different clouds) vertical velocity for shallow cumuli rather

1 than range of values that is used in the cumulus physics routine (the reasons for this
 2 simplification were discussed earlier in this sub-section). The Abdul-Razzak and Ghan
 3 (2000) parameterization provides activation fractions (f_{ACT}) for aerosol number and mass
 4 species in each size bin. The activation rate in (3) is then

$$5 \quad (\dot{q}_{ACC,U})_{ACTI} = -(\dot{q}_{AI,U})_{ACTI} = (f_{ACT}q_{AI,U})/\Delta t_U \quad (4)$$

6 where $\Delta t_U = \Delta z/w_U$ is the time for updraft air to move across a layer.

7 The wet removal rate for cloud-borne aerosol in (3) is given by

$$8 \quad (\dot{q}_{ACC,U})_{WETR} = -(f_{WETR}q_{ACC,U})/\Delta t_U \quad (5)$$

9 where f_{WETR} is the fractional removal of cloud-borne aerosols in the updraft as they move
 10 across a layer. This fractional removal is currently equal to the fractional conversion of
 11 cloud-water to precipitation across the layer, which is provided by the cumulus physics
 12 routine. Cloud water could also be converted to cloud ice in the cumulus physics routine,
 13 but currently this process is not included in the aerosol wet removal calculations. The
 14 conversion rate of cloud water to precipitation that is currently used in the cumulus
 15 physics routine is quite rapid, so in deep clouds, most cloud-borne aerosol is wet removed
 16 before reaching the detrainment level, and this simplification has little impact. However,
 17 this treatment is not ideal, and in the future, ice processes could be incorporated in the
 18 cumulus effects routine by treating cloud-ice-borne aerosol in addition to cloud-droplet-
 19 borne aerosol.

20 The aqueous-phase chemistry rate in (3) is obtained by calling the WRF-Chem cloud-
 21 chemistry routine for grid-resolved clouds (Chapman et al., 2009). This routine calculates
 22 mixing ratio changes from gas uptake and aqueous-phase reactions in an air parcel (or
 23 layer) over a specified time step, and it is applied to updraft air moving across a layer in
 24 time Δt_U .

25 For trace gases in the updraft, the continuity equation is

$$26 \quad \frac{\partial(M_U q_{G,U})}{\partial z} = \frac{(E_U q_{G,E} - D_U q_{G,U})}{\Delta z} + \rho A_U \left[(\dot{q}_{G,U})_{WETR} + (\dot{q}_{G,U})_{AQCH} \right] \quad (6)$$

1 where $q_{G,E}$ and $q_{G,U}$ are gas mixing ratios in the environment and updraft, respectively.
2 The environment gas mixing ratios are assumed equal to the grid-cell mean values, which
3 is justified given the small fractional area of the grid box covered with convective
4 updrafts. The $q_{G,U}$ includes both gas-phase and dissolved in convective cloud-water
5 species (e.g., gaseous SO_2 plus S(IV) in cloud water). The WRF-Chem cloud-chemistry
6 routine gives the aqueous-phase chemistry rate in (6), as well as the fraction of the gas
7 that is dissolved in convective cloud-water ($f_{G,CCW}$). The wet removal rate for gases only
8 considers the removal of gases dissolved in cloud droplets; and direct uptake of gases by
9 rain is currently neglected. This treatment is justified within clouds because of the
10 relatively small role of direct uptake by raindrops compared to uptake by cloud droplets
11 followed by droplet collection by rain (due to the small surface area of raindrops
12 compared to cloud drops). Also, the volume of air that moves through the updraft (and
13 experiences in-cloud wet removal) is larger than the volume that resides below cloud
14 base but does not enter the updraft (and experiences only below-cloud wet removal).
15 Future version of the parameterization will include below-cloud wet removal. The wet
16 removal rate in (6) is then

$$17 \quad (\dot{q}_{G,U})_{WETR} = -(f_{WETR} f_{G,CCW} q_{G,U}) / \Delta t_U \quad (7)$$

18 Downdrafts are assumed to be sub-saturated and contain no cloud droplets or convective-
19 cloud-borne aerosol. Thus activation, wet removal, and aqueous-phase chemistry are not
20 treated in downdrafts. The downdraft continuity equations are then

$$21 \quad \frac{\partial(M_D q_{X,D})}{\partial z} = \frac{(E_D q_{X,E} - D_D q_{X,D})}{\Delta z} \quad (8)$$

22 where X is either AI for interstitial aerosol species or G for gases.

23 Once the aerosol and gas profiles in the updraft and downdraft have been calculated,
24 conservation equations for grid-cell mean mixing ratios of aerosol and trace gas species
25 are integrated for the time sub-step. These conservation equations have the form

$$26 \quad \rho \frac{\partial \bar{q}_X}{\partial t} = -\frac{\partial}{\partial z} [M_U q_{X,U} + M_D q_{X,D} + M_E q_{X,E}] + \rho A_U [(\dot{q}_{X,U})_{ACTI} + (\dot{q}_{X,U})_{WETR} + (\dot{q}_{X,U})_{AQCH}] \quad (9)$$

1 where the X subscript is either AI , ACC , or G , and the updraft rate of change terms come
2 from the updraft calculations described above. The integration is explicit in time and uses
3 simple upstream finite differencing for the vertical transport terms. After the integration
4 sub-step, the grid-cell mean mixing ratio of convective-cloud-borne aerosol (\bar{q}_{ACC}) may
5 be non-zero at or near levels where the updraft detrains. This convective-cloud-borne
6 aerosol is partially transferred to grid-resolved cloud-borne aerosol (fraction transferred
7 equal to grid-resolved cloud fraction) and partially resuspended to interstitial aerosol. At
8 the end of all the active-cloud integration sub-steps, the new grid-cell mean aerosol and
9 gas mixing ratios reflect the effect of the active cumulus cloud over the cloud lifetime.

10 The passive cumulus effects calculations are performed next. These calculations are
11 relatively simple in comparison, as there is no vertical transport or wet removal of
12 aerosol. The cumulus physics routine provides the passive cumulus cloud fraction and
13 cloud water mixing ratio at each vertical level. Initial mixing ratios of interstitial aerosol
14 and trace gases are set equal to the grid-cell mean mixing ratios at the end of the active
15 cumulus effects calculation. Some of the interstitial aerosol is then transferred to the
16 convective-cloud-borne state, in order to provide an initial chemical composition of the
17 cloud water. For this, we assume that the cloud-borne fraction for each aerosol chemical
18 component (and size bin) is the same as the cloud-borne fraction in the steady-state
19 updraft of the active cumulus. This is conceptually consistent with the passive clouds
20 being decaying remnants of active clouds. Aqueous-phase chemistry calculations are then
21 made for this passive cloud fraction, again over the lifetime of the cumulus. Finally, the
22 passive cumulus fraction of the grid cell is mixed with the remainder of the grid cell, and
23 convective-cloud-borne aerosol is partially transferred to grid-resolved cloud-borne and
24 partially resuspended to interstitial.

25 After the passive cloud calculations, the grid-cell mean mixing ratios of aerosols and
26 trace gases reflect the effects of active and passive cumulus over the cloud lifetime.
27 These mixing ratios are returned to the host code as the updated mixing ratios. In our
28 simulations, a primary time step (for dynamics) of 15 seconds was used, and a chemistry
29 time step (for most processes involving trace gases and aerosols) of 5 minutes was used.
30 The sub-grid cumulus lifetimes, as defined within the cumulus parameterization, ranged

1 between 30 and 60 minutes, and the cumulus effects on aerosols/gases are calculated
2 once only when a cumulus is triggered in a grid column. On subsequent chemistry time
3 steps, no more cumulus effect calculations are performed until a new cumulus is triggered
4 in a column. An alternate approach would be to save the cumulus effects tendencies for
5 aerosols and gases, then apply them gradually over the cumulus lifetime, analogous to the
6 approach used in the cumulus physics for temperature, moisture, and momentum. We
7 chose this one-time update approach for aerosols and gases for simplicity and to reduce
8 memory costs associated with storing the cumulus effects tendencies for the many aerosol
9 and gas species. The net changes to the aerosol would be the same in either case, but the
10 changes are applied somewhat sooner in the once-only approach (when a cloud triggers
11 rather than over its lifetime), producing small differences in a simulation that could grow
12 over time.

13 **3 WRF-Chem configuration**

14 **3.1 Experiment setup**

15 WRF-Chem version 3.2.1 was configured in a way similar to that described by
16 Shrivastava et al. (2013). A single domain, 2240 km on a side, over the central United
17 States was used with 10 km horizontal grid spacing. WRF-Chem was also configured to
18 use 64 vertical levels, with approximately 25 levels in the lowest 1 km of the atmosphere.
19 The various parameterizations utilized in the simulations, not including the modifications
20 described in Section 2, are listed in Table 1. Multi-day WRF-Chem simulations for the
21 period of 1 June through 30 June 2007 were completed in individual 36-hour blocks. The
22 first 12 hours of each block were discarded and the final 24 hours saved for analysis.
23 Meteorological initial and boundary conditions for each block were taken from the
24 Global Forecast System (GFS). Boundary conditions of trace gases and aerosols were
25 derived from the MOZART global simulation (Emmons et al., 2010b). Initial conditions
26 for trace gases and aerosol were taken from the end of the previous simulation block.

27 Care must be taken when applying cumulus parameterizations in simulations that use an
28 intermediate grid spacing where the sub-grid scale motions can be nearly the same size as
29 the model grid size (Wyngaard, 2004) and for cases in which the assumption that the
30 updraft area in the model grid box is small (Arakawa et al., 2011). Alternative approaches

1 are being developed that include new scale aware parameterizations (e.g. Gustafson et al.,
2 2013; Grell and Freitas, 2014). In this study, the fraction of the model grid box occupied
3 by cumulus convective updrafts was analyzed and was found to generally be less than
4 10% (Figure 2). The application of the cumulus parameterization at 10 km horizontal grid
5 spacing used in this study is consistent with other work that has appeared in the literature
6 (e.g. Larson et al., 2012; Berg et al., 2013), including Gerard et al. (2009) who identified
7 horizontal grid spacing ranging from 2 to 7 km as problematic, and with
8 recommendations made in the WRF Users Guide (Skamarock et al., 2008).

9 Three sets of simulations are used to investigate the regional impacts of cloud-aerosol
10 interactions associated with both shallow and deep convection (Table 2). In all three
11 simulations, the shallow and deep cumulus physics are enabled. However, the cumulus
12 effects on aerosols and trace gases are selectively enabled in the different simulations.
13 The first simulation includes aerosol processing associated with both shallow and deep
14 clouds, and is referred to as DeepShallow. This simulation can be used to estimate the
15 regional impact on aerosol properties due to cloud processing associated with all clouds
16 in the domain (including both grid resolved and parameterized clouds). The second
17 simulation has aerosol processing by shallow convection turned on and by deep
18 convection turned off, and is referred to as ShallowOnly. The difference between
19 DeepShallow and ShallowOnly is used to document the impact of aerosol processing by
20 deep convection alone and is identified as the Deep-Effect in this work. The third
21 simulation is conducted with all aerosol processing by sub-grid convective clouds turned
22 off (Control) and is the default treatment in WRF-Chem. The difference between
23 ShallowOnly and Control simulations show the impact of shallow clouds and will be
24 identified as the Shallow-Effect in the rest of the manuscript. An additional simulation
25 was completed for a subset of the study period to document the impact of aqueous phase
26 cloud chemistry on aerosol composition. This was accomplished by repeating the
27 DeepShallow simulation for 25 June 2007 with the convective cloud aqueous chemistry
28 turned off. This run was initialized using the aerosol from the end of the previous
29 DeepShallow simulation block.

1 3.2 Emissions

2 Hourly emissions used in this study are the same as those used by Shrivastava et al.
3 (2013). In brief, hourly emissions of aerosol and trace gases are derived for the desired
4 2007 period by assuming a linear variation in the U.S. Environmental Protection
5 Agency's National Emissions Inventory (NEI; e.g.,
6 <http://www.epa.gov/ttn/chief/net/2005inventory.html>) for 2005 and 2008, supplemented
7 with biomass burning gas and aerosol emissions taken from the 2007 Fire Inventory
8 produced by NCAR (FINN07) (Wiedinmyer et al., 2011). The NEI contains two sizes of
9 particulate matter emissions: particles with diameters less than or equal to 2.5 μm ($\text{PM}_{2.5}$)
10 and those less than or equal to 10 μm (PM_{10}). NEI $\text{PM}_{2.5}$ emissions are divided into
11 categories of sulfate, nitrate, organic aerosol, elemental carbon, and unspciated primary
12 $\text{PM}_{2.5}$, following Hsu et al. (2006). As in Shrivastava et al. (2013), all unspciated $\text{PM}_{2.5}$
13 is lumped into the MOSAIC other inorganic material (OIN) category. For the simulations
14 presented here, OIN accounts for approximately 77% of the $\text{PM}_{2.5}$ mass emissions. The
15 MOZART model (Emmons et al., 2010a) was used to provide the inflow of dust through
16 the boundaries of the WRF-Chem domain with these values assumed to be OIN. $\text{PM}_{2.5}$
17 and PM_{10} emissions are mapped to eight size bins for the sectional size distribution
18 representation following Fast et al. (2006). Particles in each size bin are assumed to be
19 internally mixed and the same size distribution is assumed for all species. VOC emissions
20 were speciated using the SAPRC-99 mechanism and biogenic VOC emissions are
21 estimated using the Model of Emissions of Gases and Aerosols from Nature (MEGAN
22 <http://bai.acd.ucar.edu>) (Guenther et al., 2006). The 138 biogenic species in MEGAN are
23 grouped into three classes for use with WRF-Chem. Primary emissions are further
24 modified to account for semi-volatile and intermediate volatility organic compounds
25 (S/IVOC) that are large potential anthropogenic SOA precursors and are co-emitted with
26 primary organic aerosols (POA) (Shrivastava et al., 2008). In this study, emissions of
27 SVOC are assumed to be twice that of POA for anthropogenic sources, while IVOC
28 emissions are estimated to be 1.5 times the sum of SVOC and POA emissions, for a total
29 S/IVOC emissions equal to 6.5 times POA (Hodzic et al., 2010; Tsimpidi et al., 2010;
30 Shrivastava et al., 2011). A two-species VBS mechanism is used here, with both POA
31 and secondary organic aerosols (SOA) assumed to have a very low volatility (Shrivastava

1 et al., 2011). In previous work, Shrivastava et al. (2013) showed that this 2-species VBS
2 mechanism resulted in reasonable predictions of organic aerosols compared to
3 measurements made during CHAPS, as described in the next section.

4 **4 Data**

6 In this study, a subset of model results are compared to data collected during CHAPS,
7 which was conducted during June 2007 and included the deployment of the Department
8 of Energy's Gulfstream-1 (G-1) aircraft and National Aeronautics and Space
9 Administration (NASA) Langley Research Center B200 aircraft. During CHAPS the G-1
10 was configured for *in situ* sampling of aerosol chemical and optical properties (Berg et
11 al., 2009). The flight path was specifically designed to measure conditions below, within,
12 and above a population of shallow cumuli near Oklahoma City, Oklahoma. The size
13 distribution of aerosol and cloud drops was measured using a Droplet Measurement
14 Technology (DMT) Passive Cavity Aerosol Spectrometer Probe (PCASP) and DMT
15 Cloud Aerosol Spectrometer (CAS). The G-1 was equipped with two aerosol inlets: an
16 isokinetic inlet for sampling aerosol in clear air and interstitial aerosol within clouds, and
17 a Counter Flow Virtual Impactor (CVI) to sample only cloud droplets. An Aerodyne
18 Aerosol Mass Spectrometer (AMS) was used to analyze the composition of non-
19 refractory aerosol sampled via both inlets. In their work, Shrivastava et al. (2013)
20 evaluated the performance of WRF-Chem for the same period and found reasonable
21 agreement with the observations when the model was run with relatively fine spatial
22 resolution that explicitly represented convection. They reported some discrepancies
23 between the simulated and observed aerosol optical properties, but these were attributed
24 to assumptions related to the emissions, hygroscopicity, and complex index of refraction
25 of of OIN particles, in addition to aerosol water content.

26 The B200 was equipped with the downward looking NASA Langley high spectral
27 resolution lidar (HSRL-1) that provided height resolved observations of aerosol
28 backscatter, extinction, and depolarization that were nearly simultaneous with the *in situ*
29 G-1 measurements. Details of the HSRL-1 system can be found in Hair et al. (2008). The
30 HSRL-1 uses the spectral distribution of the lidar return signal to separate the molecular

1 and aerosol signal and can independently determine the aerosol backscatter, extinction,
2 and depolarization at a wavelength of 532 nm. The HSRL-1 also functions as a standard
3 backscatter lidar at a wavelength of 1064 nm, measuring both backscatter and
4 depolarization at that wavelength. During CHAPS, the B200 aircraft flew above the G-1,
5 providing lidar “curtains” along the flight track.

6 **5 Analysis**

7 In a previous case study, Berg et al. (2013) showed that the use of the KF-CuP
8 parameterization in WRF led to a significant increase in the amount of simulated shallow
9 sub-grid convective clouds for three days in 2007 (16 May, 2 July, and 24 July) over the
10 Department of Energy’s Atmospheric Radiation Measurement (ARM) Central Facility,
11 consistent with observations. Therefore, the performance of the cumulus parameterization
12 will not be rigorously evaluated here. A single example of the model’s ability to simulate
13 the observed cloud fields is illustrated in Figure 2 that shows the GOES visible image
14 (valid at 20:15 UTC) and the cloud fraction associated with sub-grid clouds simulated by
15 the cumulus parameterization and areas with grid resolved clouds at 20:00 UTC on 25
16 June 2007. The KF-CuP parameterization predicts large areas with shallow convection
17 over much of the central United States, which is consistent with the areas of shallow
18 cumuli seen in the satellite image over much of Iowa, Kansas and Missouri, and a
19 number of deep convective clouds over Texas and Oklahoma. The frequency of
20 occurrence in which shallow or deep convection were triggered in the WRF grid columns
21 for the period 12:00-20:00 UTC on 25 June 2007 is shown in Figure 3 and provides
22 information about the air-mass history in regards to sub-grid cumuli within the three
23 boxes. Note that there can be cases in which the color shading indicates both shallow and
24 deep clouds in the same model grid column. This occurs when different cloud types occur
25 at different times of day.

26 Due to the spatial inhomogeneity of the cloud fields over the central United States
27 highlighted in Figure 2, our analysis of conditions on 25 June will focus on three different
28 distinct regions each approximately 240 km on a side, not just the CHAPS area around
29 Oklahoma City that was analyzed by Shrivastava et al. (2013). These areas,
30 approximately centered on Madison, Wisconsin (MSN); Austin, Texas (AUS); and

1 Oklahoma City, Oklahoma (OKC), were selected because they contain primarily shallow
2 convection (MSN), deep convection (AUS), or a mixture of both (OKC) (see Figure 3)
3 and allow us to better understand the behavior of the model and its parameterizations
4 over a range of conditions. The MSN box has a very high frequency of shallow clouds
5 distributed over the box with the nearest up-stream deep convection occurring over
6 central Illinois. The AUS box has a very small frequency of simulated sub-grid shallow
7 clouds and a much larger frequency of simulated sub-grid deep convective clouds. In
8 contrast to the other two boxes, the OKC box includes a mixture of both shallow and
9 deep convection.

10 While MOSAIC represents multiple aerosol constituents, only BC, OA, and sulfate have
11 been selected for analysis within the three boxes. These particular constituents were
12 selected because of their climatic relevance, and their representative behavior. BC is, to a
13 first approximation, only impacted by transport, activation/resuspension, dry deposition,
14 and wet removal—and in the case of non-precipitating convection acts essentially as a
15 passive tracer. Although freshly emitted BC is hydrophobic, the internal mixing
16 assumption applied in the model causes it to quickly reside in hygroscopic particles.
17 Interpretation of cloud-aerosol interactions and vertical sulfate transport is more
18 complicated than for BC because sulfate can be produced within cloud droplets via
19 aqueous-phase oxidation of dissolved sulfur dioxide gas as well as removed via
20 precipitation (e.g. Koch et al., 2003). While the majority of OA in the atmosphere is
21 secondary and is somewhat hygroscopic, its behavior within convective clouds is similar
22 to that of BC aerosol because the aqueous chemistry related to OA production is not fully
23 understood and currently is not included in the model.

24 **5.1.1 Local Impacts on Aerosol Vertical Distribution**

25 One important impact of convective clouds is the vertical redistribution of aerosol due to
26 the impact of convective updrafts, downdrafts, entrainment mixing, enhanced subsidence,
27 and wet removal associated with sub-grid clouds. Figure 4 shows examples of vertical
28 north-south cross sections (through the center of the analysis boxes) of the amount of BC
29 (including both interstitial and activated aerosol in the cloudy grid cells) for the
30 DeepShallow case and the fractional change in BC loading between the DeepShallow and

1 control simulations (indicated by the colors) as well as the cloud fraction (indicated by
2 the gray shading) within the AUS and MSN boxes valid at 20:00 UTC on 25 July, 2007.
3 Within both the AUS and MSN boxes the largest BC mass loadings are found near the
4 surface. There are also large amounts of BC 4-6 km above the surface in the AUS cross
5 section that is apparent in both the DeepShallow (Figure 4) and Control simulations (not
6 shown). This elevated layer is not associated with convection but rather with long-range
7 transport, most likely from a fire located central in New Mexico (not shown) and a coal-
8 fired power plant in Colorado.

9 At first glance it might be surprising that there are not columns of enhanced aerosol
10 loading within the AUS clouds due to enhanced upward transport from the sub-cloud
11 layer shown in Figure 4. Their absence is primarily due to the wet removal of aerosol
12 within the lowest levels of the clouds, as well as the cloud fraction (which ranges from 20
13 to 60% within the deep convective clouds shown in the figure), which reduces the
14 relative impact of the aerosol in the updraft, within any given model grid cell. In the AUS
15 cross section, the large fractional increase in BC between the DeepShallow and Control
16 simulations for altitudes ranging from 3 and 5 km and the decrease above 5 km can be
17 attributed to vertical transport by updrafts, downdrafts, and convection induced
18 subsidence. At these altitudes (which are below the detrainment level), this transport
19 replaces some of the air (and aerosol) in a grid cell with air from higher levels that has
20 smaller BC concentrations.

21 Within the AUS cross section, the clouds extend from an altitude of approximately 0.5
22 km to nearly 15 km. The clouds in the MSN box are much shallower, extending from
23 approximately 1 to 2 km as is more typical for boundary-layer cumuli (e.g. Berg and
24 Kassianov, 2008). The decrease in amount of BC loading in the sub-cloud layer is caused
25 by the venting of aerosol out of that layer by the convective clouds. In contrast to the
26 AUS box that includes deep sub-grid convective clouds, the vertical extent of the
27 transport of BC is more limited within the MSN box (Figure 4b). This result is consistent
28 with the much smaller vertical extent of the clouds in this box. Within the cloud layer, the
29 shallow cumuli still have an important impact on the vertical extent of the BC (Figure
30 4d). The fractional difference in the BC between the DeepShallow and Control
31 simulations approaches 50% as the convective clouds transport BC from below the cloud

1 into the cloud layer. The net effect of the non-precipitating cumuli is to mix BC over the
2 sub-cloud and cloud layers.

3 Similar to the case for BC, there is an elevated plume of sulfate aerosol near an altitude of
4 5 km in the AUS cross-section that is associated with long-range transport (Figure 5a). In
5 both the AUS and MSN cross-sections there is a large concentration of sulfate within the
6 boundary layer that is associated with surface emissions. As with BC, fractional
7 differences between the DeepShallow and Control runs are much larger than 50%. Within
8 the AUS box there is a large fractional change in the amount of sulfate aloft that can be
9 attributed to vertical transport by updrafts, downdrafts, and convection induced
10 subsidence that are represented in the DeepShallow simulations (Figure 5c). The situation
11 is different in the MSN box, where all of the clouds are shallow non-precipitating cumuli
12 (Figure 5b and d). In this case, the vertical transport is limited to the cloud layer (altitudes
13 lower than approximately 2 km), where there is significant increase in the sulfate loading
14 in the cloud layer (Figure 5b). In contrast to the BC within the MSN box, the sulfate is
15 enhanced in the ShallowOnly simulations both below and within the cloud layer. This is
16 due to sulfate production within clouds, the detrainment of cloudy air with enhanced
17 sulfate, and subsequent downward transport of air back into the subcloud layer. There is
18 no evidence of lofted sulfate in the levels above the shallow cumuli (Figure 5b).

19 Using data from the G-1 aircraft alone, it is difficult to verify the simulation of the
20 vertical transport of aerosol associated with cumulus. Data from the airborne NASA
21 HSRL, however, can be used to investigate the vertical extent of aerosol in the vicinity of
22 convective clouds. This data set does not provide information in regards to the speciation
23 of the aerosol, but it can be used to look at impacts on the aerosol backscatter and
24 extinction, which are highly correlated with the aerosol loading. Unfortunately, HSRL
25 data are not available for 25 June, so two other days have been selected for analysis of
26 vertical transport, including 19 and 21 June 2007. The frequency of simulated shallow
27 and deep clouds are shown in Figure 6, and both days had relatively large amounts of
28 simulated shallow clouds both before and during the G-1 and B200 flights.

29 Conditions on 19 June were marked by large amounts of both observed and simulated
30 shallow cumuli near Oklahoma City and are similar to the MSN grid box on 25 June. In

1 most cases the observed shallow cumuli are sufficiently optically thick that the laser
2 beam is attenuated by the cloud, leading to the frequent periods of missing data below
3 cloud top (as indicated by the white areas underneath peaks in the aerosol backscatter in
4 Figure 7). On 19 June the majority of cloud-top heights measured by the HSRL are found
5 to range from 1 to 2.5 km and there are relatively large amounts of aerosol backscatter
6 and extinction from the surface to an altitude of 2.5 km, which roughly corresponds to the
7 highest cloud top heights observed during the B200 flight. The DeepShallow and Control
8 simulations were subsampled along the B200 flight track and the fractional difference in
9 the WRF-Chem simulated extinction and cloud fraction associated with convective
10 clouds is shown in Figure 7c. Both the DeepShallow and Control simulations
11 underestimate the aerosol extinction on 19 June by approximately a factor of 1.25 to 2.0
12 compared to the values derived from the HSRL (not shown). This is likely due to issues
13 with the simulated mass loading as well as simulated water uptake by the aerosol. Given
14 that both sets of simulations underestimate the observed values, the underestimate of
15 backscatter and extinction is not attributable to the treatment of sub-grid convective
16 clouds. The simulated cloud fraction reaches values as large as 40% and the vertical
17 extent of the simulated clouds is consistent with the HSRL observations. The largest
18 positive differences in the simulated extinction are associated with the layer of shallow
19 cumuli. The enhanced transport associated with the DeepShallow simulations spread the
20 aerosol, and hence aerosol extinction, over a layer from the surface to an altitude of 2 km,
21 compared to only 1 km in the control simulations. The values of extinction in the
22 DeepShallow simulations are 10-20% greater over altitudes ranging from 1 to 2 km than
23 was found in the Control simulations, while the extinction in the subcloud layer is
24 reduced by a similar magnitude. This behavior is similar to the changes in the seen with
25 the BC loading within the MSN analysis box on 25 June (Figure 4).

26 In contrast to 19 June, which had a large fraction of shallow convection and very few
27 deep clouds near Oklahoma City, conditions on 21 June were marked by a mixture of
28 deep and shallow clouds in both the observations and simulations. The HSRL data shows
29 a region of higher clouds (near 20:00 UTC; Figure 8). The tops of the observed shallow
30 clouds range from approximately 1 to 2 km and are distributed along much of the entire
31 flight track. The vertical transport associated with the clouds leads to enhanced aerosol

1 backscatter and extinction to an altitude of 2 km. There are fewer simulated clouds along
2 the flight track at the time of the B200 flights than is observed, and there are some
3 simulated deep convective clouds between 19:30 and 20:00 UTC and near 21:15 UTC
4 (Figure 8). There are some systematic changes in the simulated aerosol extinction,
5 suggesting additional clouds upwind of the flight track, or clouds that occur before the
6 B200 was aloft. These changes include an increase in the aerosol extinction in the
7 DeepShallow simulations near an altitude of 1.75 km between 19:00 to nearly 20:00
8 UTC, and near an altitude of 2 km from 20:15 through approximately 21:30 UTC. The
9 results for 21 June are reminiscent of changes seen in the AUS analysis box for 25 June
10 and suggest an increased impact of deep convection on 21 June than was seen on 19 June.

11 **5.2 Regional scale impacts**

12 The results presented in Section 5.1 highlight that the parameterization is performing
13 reasonably and can be used to investigate the regional impacts of cloud-aerosol
14 interactions within the areas defined by the analysis boxes. The primary advantage of
15 using a parameterization to represent convective clouds is the ability to run simulations
16 over a large domain, which enables the evaluation of regional scale impacts of cloud-
17 aerosol interactions on the aerosol lifecycle that is not possible using high-resolution
18 simulations. Differences in the column-integrated mass loading are one method that can
19 be used to investigate changes in mass loading of atmospheric aerosol over large areas.
20 BC represents particles that are essentially passive tracers (ignoring wet and dry removal)
21 that do not undergo aqueous phase chemistry in simulated clouds. Overall, there is a
22 significant reduction in the column integrated BC and OA across the model domain
23 (Figure 9). The primary removal mechanism added in the DeepShallow simulations
24 (compared to the Control simulations) is the wet removal associated with the
25 parameterized precipitation. This leads to systematic decreases of as much as -50% in the
26 amount of BC. It is interesting to note that there is a net decrease of BC within the MSN
27 box in which there is no convection and very little grid resolved precipitation, indicative
28 of wet removal upwind of the box during the simulation and pointing to regional scale
29 impacts of cloud-aerosol interactions. There are also small areas in which the column
30 integrated BC loading is larger in the DeepShallow than control simulations. These

1 features are also present in the ShallowOnly case (not shown). The increase in the
2 column integrated BC in the AUS box is the result of slight differences in the path of the
3 aerosol plume coming from the Houston, Texas area. Different aerosol loadings in the
4 simulations produce different feedbacks on meteorology (i.e.. aerosol indirect effects in
5 grid-resolved clouds and aerosol direct effects), leading to small differences in winds. In
6 the DeepShallow simulations the main part of the plume is shifted a small distance to the
7 north, giving rise to the apparent increase in the BC loading just downwind of Houston.

8 The OA follows a pattern similar to what is seen for BC, but the fractional change is
9 smaller in magnitude. Currently in WRF-Chem the OA are unaffected by aqueous
10 chemistry within the clouds, but can be affected by changes in the amount of precursor
11 gases. Vertical transport of SOA precursor gases (which are not wet-removed in our
12 parameterization) to higher and colder altitudes can result in more partitioning to the
13 particle phase. These changes lead to areas, such as the central swath through the OKC
14 box, and over parts of the southeastern United States, where there is an increase in the
15 column integrated OA. Based on these simulations the change in OA can be significant,
16 approaching a column integrated increase of 10 to 15% for some areas.

17 In contrast to BC, the wet removal of sulfate can be counteracted by its production in
18 cloud. In the AUS box, sulfate wet removal is larger than production, leading to a small
19 net decrease in sulfate when cloud-aerosol interactions (including aqueous chemistry)
20 associated with deep and shallow clouds are considered. Within the MSN box (and over
21 much of the upper-midwest), there is no convective and very little grid resolved
22 precipitation so that the production of sulfate aerosol by aqueous chemistry dominates
23 and there is a significant increase in the column burden of sulfate when non-precipitating
24 clouds are present (Figure 9). The additional sulfate is limited to the cloud layer and
25 below, but as shown in Figure 5 this enhanced sulfate can spread over a deeper layer of
26 the atmosphere. Relative to the control case where the impacts of cumulus are ignored,
27 our results indicate that cumulus can increase the column sulfate burden by as much as
28 40%. While the simulations shown here were rather short, longer integration times could
29 lead to significant differences downwind of the area of sulfate production due to
30 enhanced vertical mixing and regional scale transport.

1 **5.3 Impact on cloud microphysics**

2 Using data collected during CHAPS, Berg et al. (2011) measured differences in cloud
3 microphysical properties as a result of differences in the amount of aerosol within
4 individual clouds and the cloud draft velocity. They used perturbation of CO (CO';
5 defined as the difference between the instantaneous measured CO and the average CO
6 observed during a flight leg) as an indicator of increased aerosol. They found systematic
7 increases in the cloud droplet number concentration (CDNC) associated with both
8 increases in CO' and the cloud updraft strength, which highlighted the importance of
9 considering both the aerosol loading and the cloud dynamics. In their analysis of high-
10 resolution WRF-Chem simulations, Shrivastava et al. (2013) found results consistent with
11 those reported by Berg et al. (2011). A similar analysis has been completed here using
12 results from the DeepShallow simulations in the OKC analysis box, but limited to only
13 grid columns with shallow convection. The cloud microphysical properties were
14 computed for only the cloudy updrafts, as this is the part of the parameterized clouds
15 where the sub-cloud particle loading can influence the cloud microphysical properties via
16 drop activation. A probability density function (PDF) of simulated CO' and perturbation
17 vertical velocity (w' , defined in a way analogous to CO') is shown in Figure 10. In this
18 case the parameterized updraft speeds were found to range from 1.0 to 3.5 m s⁻¹ which
19 are consistent with the updraft speeds in Figure 1 of Berg et al. (2011).

20 For the parameterized sub-grid convective clouds the CDNC is found to increase with
21 increasing values of CO, showing an increase from about 500 to 800 cm⁻³ (an increase by
22 about a factor of 1.6) as the CO' ranges from clean (-35 ppbv) to dirty (+35 ppbv) for
23 model grid cells where the updraft ranges from 2.0 to 2.5 ms⁻¹ (Figure 10). The results are
24 fairly noisy with relatively large standard deviations highlighting the wide range of
25 additional factors that can impact the CDNC. The slope of the CDNC vs. CO' regression
26 line for w' equal to 2.0-2.5 m s⁻¹ is computed to be 4.2 cm⁻³ ppbv⁻¹, which is smaller than
27 the 7.2 cm⁻³ ppbv⁻¹ reported by Berg et al. (2011), but is close to the value of 4.5 cm⁻³
28 ppbv⁻¹ derived from the results of Shrivastava et al. (2013). The different slopes seen in
29 the observations, those reported by Shrivastava et al. (2013) and this study could be
30 related to the smoothing of emissions, which has been documented in the literature in
31 regards to both simulated cloud characteristics (Gustafson et al., 2007) and aerosol

1 loadings (Gustafson et al., 2011). The results shown by the different studies should be
2 considered with care, however, because of the different vertical velocity ranges used in
3 each case. While not ideal, the different w ranges were applied because of differences in
4 the spatial and temporal scales associated with the observations and high- and low-
5 resolution simulations.

6 **5.4 Chemical composition of cloud drops**

7 Changes to chemical properties of the particles associated with passage through clouds
8 are an important aspect of cloud aerosol interactions. One of the goals of the CHAPS
9 study was to document changes in the chemical composition of particles that served as
10 CCN (activated) or remained inactive (interstitial). During CHAPS, measurements
11 showed both the activated and interstitial aerosol were dominated by organics and sulfate
12 (Figure 11). In their analysis, Berg et al. (2009) also reported enhanced nitrate in the
13 dried cloud drop residuals that were sampled via a counter flow virtual impactor (CVI).
14 They attributed this to the uptake of gas-phase nitric acid by cloud drops. In their analysis
15 of high-resolution WRF-Chem simulations, Shrivastava et al. (2013) also found enhanced
16 nitrate when aqueous phase chemistry, which includes trace gas-liquid phase equilibria,
17 was turned on. When aqueous phase chemistry was turned off, however, the particle
18 nitrate in cloud drop residuals and interstitial particles was nearly the same, indicating the
19 importance of the uptake and dissociation of gas-phase nitric acid within cloud drops.

20 A similar analysis has been completed for the OKC box using results from ShallowOnly
21 simulations. The mass loading of the interstitial aerosol within the shallow clouds is
22 generally smaller in this study than the loading reported by Shrivastava et al. (2013) for
23 either the observations (Figure 11) or high-resolution simulations (Figure 7 of
24 Shrivastava et al., 2013). This behavior may, in part, be attributed to the averaging of the
25 emissions over the larger model grid cell in the vicinity of Oklahoma City and the
26 location of the simulated shallow clouds in the two studies. In contrast to the interstitial
27 particles, the simulated mass loading of the activated aerosol is larger in all three
28 simulations (grid-resolved, ShallowOnly with cloud chemistry on, and ShallowOnly with
29 cloud chemistry off) than the loading that was observed during CHAPS. The over-
30 estimation of simulated aerosol mass may, in part, be due to the cut size used by the CVI

1 operated on the aircraft that would exclude small cloud drops. In contrast to the aerosol
2 mass loading, the observed and simulated aerosol volume fractions are in good
3 agreement. Thus, even if the mass loading is incorrect, the consistent volume fractions
4 indicates that the chemical processing within the model clouds is behaving in a way that
5 is consistent with the observations. Similar to the observations and high-resolution
6 simulations, there is an increase in the volume fraction of nitrate in activated (cloud-
7 borne) aerosol compared to interstitial aerosol.

8 The analysis of activated versus interstitial aerosol composition is repeated for the
9 CHAPS flights on 20 and 23 June. These days also had shallow cumuli in the vicinity of
10 Oklahoma City, although the simulated cloud fraction (not shown) was less than was seen
11 on 19, 21, and 25 June. On 20 June, the median organic volume fractions of interstitial
12 aerosol were approximately 75% organics and 15% sulfate, with small amounts of nitrate
13 and ammonium (Figure 12a). The activated aerosol sampled using the CVI were also
14 dominated by organics, but there was a great deal of variability in the volume fraction of
15 organics as well as an increase in the volume fraction of nitrate. The ShallowOnly
16 simulations for the OKC box for 20 June are consistent with the observed values and
17 follow the same trends for both interstitial and activated aerosol. The variability in the
18 simulated volume fraction is much less than was observed, which could be a result of the
19 relative small amount of simulated sub-grid convective clouds on that day. The simulated
20 activated aerosol also had enhanced values of nitrate aerosol compared to the interstitial
21 aerosol. Observations on 23 June include a smaller volume fraction (60%) of organics in
22 the case of interstitial aerosol, and increased volume fraction of sulfate (30%) compared
23 to the other two days (Figure 11 and Figure 12b). The volume fraction of activated
24 aerosol is also dominated by organics, but like conditions on 20 June, there is a great deal
25 of variability. The ShallowOnly simulations have a relatively large median volume
26 fraction associated with sulfate aerosol that is consistent with observations and smaller
27 amounts of organic aerosol than was seen on 20 and 25 June. The simulations also have
28 enhanced nitrate volume fraction compared to the interstitial aerosol. Thus the increase in
29 nitrate aerosol seen in both the observations and simulations associated with aqueous
30 chemistry is not limited to a single day, but rather is found to be a relatively common
31 occurrence in the OKC box during CHAPS.

1 **Summary and Conclusions**

2 A new treatment of cloud-aerosol interactions within parameterized shallow and deep
3 convection has been implemented in WRF-Chem with the goal of improving regional
4 scale simulations of the aerosol lifecycle and cloud-aerosol interactions. The
5 modifications designed to represent cloud-aerosol interactions include treatment of the
6 cloud droplet number mixing ratio; key cloud microphysical and macrophysical
7 parameters (including the updraft fractional area, updraft and downdraft mass fluxes, and
8 entrainment) averaged over the population of shallow clouds, or a single deep convective
9 cloud; and vertical transport, activation/resuspension, aqueous chemistry, and wet
10 removal of aerosol and trace gases in warm clouds. These changes have been
11 implemented in the WRF-Chem chemistry package as well as the Kain-Fritsch cumulus
12 parameterization (Kain and Fritsch, 1990; Kain, 2004), which has been modified to better
13 represent shallow convective clouds (Berg et al., 2013). Results from simulations using
14 the new version of WRF-Chem are compared with data from the CHAPS field
15 experiment (Berg et al., 2009; Berg et al., 2011) as well as high-resolution simulations
16 (Shrivastava et al., 2013).

17 The results are encouraging and demonstrate the advantages of the modifications that
18 have been made to WRF-Chem. It is shown that both deep and shallow convective clouds
19 have an important impact on the horizontal and vertical distribution of aerosol loading.
20 Three different domain sub-regions were selected for detailed analysis, including
21 locations near Madison, Wisconsin (MSN), Austin, Texas (AUS), and Oklahoma City,
22 Oklahoma (OKC), the latter corresponding to the site of CHAPS and the domain used in
23 previous high-resolution simulations. These regions were selected to represent instances
24 dominated by shallow (MSN), deep (AUS), or a mix of both (OKC) types of convective
25 clouds. In each case the WRF-Chem simulations behaved in a manner consistent with
26 expectations and consistent with both the CHAPS data and the results of high-resolution
27 simulations. In the case of shallow clouds, enhanced mixing leads to a deepening of the
28 layer containing BC and decreased amounts of BC near the surface. Results are similar
29 for OA, but the net impact was found to be smaller. In contrast to BC, sulfate aerosol was
30 enhanced throughout the layer due to sulfate production within clouds. In the vicinity of
31 AUS, the impact of shallow convective clouds is minimal. There was a decrease in BC,

1 OA, and sulfate in the sub-cloud layer due to vertical transport associated with deep
2 convective clouds. There were also significant changes in the aerosol loading aloft that
3 were the result of the impacts of updrafts, downdrafts, entrainment mixing, enhanced
4 subsidence, and wet removal associated with the sub-grid clouds. In the area near OKC,
5 both the deep and shallow sub-grid convective clouds had a significant impact on the
6 simulated aerosol loading. The shallow sub-grid clouds led to a decrease of aerosol in the
7 sub-cloud layer and an increase of aerosol aloft. The parameterized deep-convective
8 clouds led to decreases in the BC and OA over the lowest 2 km and sulfate over the
9 lowest 3 km of the atmosphere.

10 One of the motivations for the development of the improved parameterization is to allow
11 the investigation of regional and synoptic scale aerosol transport. In our case-study
12 period, there is a significant reduction in the BC and OA over much of the central United
13 States. The primary removal mechanism added in the new treatment is the wet removal
14 associated with the parameterized precipitation. Thus, the differences in the aerosol
15 loading highlight the importance of wet removal on the aerosol lifecycle at the regional
16 scale. In contrast to BC and OA, there are large regions in which there are increases in
17 the column-integrated sulfate due to the production of sulfate and absence of wet removal
18 in nonprecipitating clouds.

19 The behavior of the modified version of WRF-Chem in regards to the cloud
20 microphysical properties and chemical composition of aerosol is also investigated. The
21 results show that the modified version of WRF-Chem is able to reproduce changes in the
22 cloud droplet number concentration in a way that is consistent with both high-resolution
23 simulations and observations from CHAPS. The CDNC associated with the
24 parameterized clouds was found to be less sensitive to pollutant loading than was
25 observed (Berg et al., 2011) but was similar to that reported by Shrivastava et al. (2013)
26 in their high resolution simulations. The chemical composition of the simulated cloud-
27 drop residuals is compared to the composition measured with an AMS operated behind a
28 CVI inlet during CHAPS. While there were differences in the simulated and observed
29 mass loadings, the simulated and observed mass fractions were consistent, including the
30 presence of enhanced amounts of nitrate in the cloud drop residuals. WRF-Chem is also
31 able to accurately represent the increase in nitrate found in the observed cloud-drop

1 residuals. Overall, these findings provide evidence that the modified version of WRF-
2 Chem is able to represent key features of the cloud-aerosol interactions in a realistic way.
3 While the results presented here utilized WRF-Chem version 3.2.1, the code is being
4 ported to the latest version of WRF-Chem and we anticipate including these changes in a
5 future public release of WRF-Chem.

6

7 **Acknowledgements**

8 This research was supported by the Office of Science of the U.S. Department of Energy
9 as part of the Atmospheric System Research Program (ASR). The Pacific Northwest
10 National Laboratory is operated by Battelle Memorial Institute under contract DE-AC06-
11 76RLO 1830. The funding for the B200 and HSRL operations came from the NASA
12 Science Mission Directorate, the Department of Energy ASR program, and the NASA
13 CALIPSO project. The authors would also like to thank the NASA Langley King Air B-
14 200 and DOE G-1 flight crews for their outstanding work supporting these flights and
15 measurements. Drs. J. Ogren of NOAA and E. Andrews of the Cooperative Institute for
16 Research in Environmental Sciences (CIRES) deployed the CVI during CHAPS. Data
17 from the AMS was collected by Drs. Y.-N. Lee of Brookhaven National Laboratory
18 (BNL), M. L. Alexander of Pacific Northwest National Laboratory and J. Jayne of
19 Aerodyne. Size distribution data were provided by Dr. G. Senum of BNL. Drs. G. Grell
20 (NOAA) and R. Leung (PNNL) provided feedback on various aspects of the manuscript.
21

1

2 **6 References**

3 Abdul-Razzak, H., and Ghan, S. J.: A parameterization of aerosol activation 2. Multiple
4 aerosol types, *J. Geophys. Res.*, 105, 6837-6844, 10.1029/1999jd901161, 2000.

5 Ahmadov, R., McKeen, S. A., Robinson, A. L., Bahreini, R., Middlebrook, A. M., de
6 Gouw, J. A., Meagher, J., Hsie, E. Y., Edgerton, E., Shaw, S., and Trainer, M.: A
7 volatility basis set model for summertime secondary organic aerosols over the eastern
8 United States in 2006, *J. Geophys. Res.*, 117, D06301, 10.1029/2011jd016831, 2012.

9 Alapaty, K., Herwehe, J. A., Otte, T. L., Nolte, C. G., Bullock, O. R., Mallard, M. S.,
10 Kain, J. S., and Dudhia, J.: Introducing subgrid-scale cloud feedbacks to radiation for
11 regional meteorological and climate modeling, *Geophys. Res. Lett.*, 39, L24809,
12 10.1029/2012gl054031, 2012.

13 Arakawa, A., Jung, J. H., and Wu, C. M.: Toward unification of the multiscale modeling
14 of the atmosphere, *Atmos. Chem. Phys.*, 11, 3731-3742, 10.5194/acp-11-3731-2011,
15 2011.

16 Barahona, D., and Nenes, A.: Parameterization of cloud droplet formation in large-scale
17 models: Including effects of entrainment, *J. Geophys. Res.*, 112, 10.1029/2007jd008473,
18 2007.

19 Berg, L. K., and Stull, R. B.: Parameterization of Joint Frequency Distributions of
20 Potential Temperature and Water Vapor Mixing Ratio in the Daytime Convective
21 Boundary Layer, *J. Atmos. Sci.*, 61, 813-828, 10.1175/1520-
22 0469(2004)061<0813:pojfd>2.0.co;2, 2004.

23 Berg, L. K., and Stull, R. B.: A Simple Parameterization Coupling the Convective
24 Daytime Boundary Layer and Fair-Weather Cumuli, *J. Atmos. Sci.*, 62, 1976-1988,
25 10.1175/jas3437.1, 2005.

26 Berg, L. K., and Kassianov, E. I.: Temporal Variability of Fair-Weather Cumulus
27 Statistics at the ACRF SGP Site, *J. Climate*, 21, 3344-3358, 10.1175/2007jcli2266.1,
28 2008.

29 Berg, L. K., Berkowitz, C. M., Hubbe, J. M., Ogren, J. A., Hostetler, C. A., Ferrare, R.
30 A., Hair, J. W., Dubey, M. K., Mazzoleni, C., Andrews, E., Coulter, R. L., Lee, Y.-N.,
31 Olfert, J., and Springston, S. R.: Overview of the Cumulus Humilis Aerosol Processing
32 Study, *Bull. Amer. Meteor. Soc.*, 90, 1653-1667, 10.1175/2009bams2760.1, 2009.

33 Berg, L. K., Berkowitz, C. M., Barnard, J. C., Senum, G., and Springston, S. R.:
34 Observations of the first aerosol indirect effect in shallow cumuli, *Geophys. Res. Lett.*,
35 38, 10.1029/2010gl046047, 2011.

- 1 Berg, L. K., Gustafson, W. I., Kassianov, E. I., and Deng, L.: Evaluation of a Modified
2 Scheme for Shallow Convection: Implementation of CuP and Case Studies, *Mon. Wea.*
3 *Rev.*, 141, 134-147, 10.1175/mwr-d-12-00136.1, 2013.
- 4 Boucher, O., Randall, D. A., Artaxo, P., Bretherton, C. S., Feingold, G., Forster, P.,
5 Kerminen, V.-M., Kondo, Y., Liao, H., Lohmann, U., Rasch, P., Satheesh, S. K.,
6 Sherwood, S., Stevens, B., and Zhang, X. Y.: Clouds and Aerosols, in: *Climate Change*
7 *2013: The Physical Science Basis. Contribution of Working Group I to the Fifth*
8 *Assesment Report to the Intergovernmental Panel on Climate Change*, edited by: Stocker,
9 T. F., Qin, D., Plattner, G.-K., Tignor, M., Allen, S. K., Boschung, J., Nauels, A., Xia, Y.,
10 Bex, V., and Midgley, P. M., Cambridge University Press, Cambridge, United Kingdom
11 and New York, NY, USA, 2013.
- 12 Carter, W. P. L.: SAPRC-99 Mechanism Files and Associated Programs and Examples:
13 <http://www.cert.ucr.edu/~carter/SAPRC99/>, last updated March 30, 2010, 2010.
- 14 Chapman, E. G., Gustafson Jr, W. I., Easter, R. C., Barnard, J. C., Ghan, S. J., Pekour, M.
15 S., and Fast, J. D.: Coupling aerosol-cloud-radiative processes in the WRF-Chem model:
16 Investigating the radiative impact of elevated point sources, *Atmos. Chem. Phys.*, 9, 945-
17 964, 10.5194/acp-9-945-2009, 2009.
- 18 Chen, F., Mitchell, K., Schaake, J., Xue, Y., Pan, H.-L., Koren, V., Duan, Q. Y., Ek, M.,
19 and Betts, A.: Modeling of land surface evaporation by four schemes and comparison
20 with FIFE observations, *J. Geophys. Res.*, 101, 7251-7268, 10.1029/95jd02165, 1996.
- 21 Collins, W. D., Rasch, P. J., Boville, B. A., Hack, J. J., McCaa, J. R., Williamson, D. L.,
22 Kiehl, J. T., Briegleb, B., Bitz, C., Lin, S.-J., Zhang, M., and Dai, Y.: Description of the
23 NCAR Community Atmosphere Model (CAM 3.0), 2004.
- 24 Emmons, L. K., Apel, E. C., Lamarque, J. F., Hess, P. G., Avery, M., Blake, D., Brune,
25 W., Campos, T., Crawford, J., DeCarlo, P. F., Hall, S., Heikes, B., Holloway, J., Jimenez,
26 J. L., Knapp, D. J., Kok, G., Mena-Carrasco, M., Olson, J., O'Sullivan, D., Sachse, G.,
27 Walega, J., Weibring, P., Weinheimer, A., and Wiedinmyer, C.: Impact of Mexico City
28 emissions on regional air quality from MOZART-4 simulations, *Atmos. Chem. Phys.*, 10,
29 6195-6212, 10.5194/acp-10-6195-2010, 2010a.
- 30 Emmons, L. K., Walters, S., Hess, P. G., Lamarque, J. F., Pfister, G. G., Fillmore, D.,
31 Granier, C., Guenther, A., Kinnison, D., Laepple, T., Orlando, J., Tie, X., Tyndall, G.,
32 Wiedinmyer, C., Baughcum, S. L., and Kloster, S.: Description and evaluation of the
33 Model for Ozone and Related chemical Tracers, version 4 (MOZART-4), *Geosci. Model*
34 *Dev.*, 3, 43-67, 10.5194/gmd-3-43-2010, 2010b.
- 35 Fan, J., Leung, L. R., Li, Z., Morrison, H., Chen, H., Zhou, Y., Qian, Y., and Wang, Y.:
36 Aerosol impacts on clouds and precipitation in eastern China: Results from bin and bulk
37 microphysics, *J. Geophys. Res.*, 117, n/a-n/a, 10.1029/2011jd016537, 2012.
- 38 Fast, J. D., Gustafson, W. I., Jr., Easter, R. C., Zaveri, R. A., Barnard, J. C., Chapman, E.
39 G., Grell, G. A., and Peckham, S. E.: Evolution of ozone, particulates, and aerosol direct

1 radiative forcing in the vicinity of Houston using a fully coupled meteorology-chemistry-
2 aerosol model, *J. Geophys. Res.*, 111, D21305, 10.1029/2005jd006721, 2006.

3 Gerard, L., Piriou, J.-M., Brožková, R., Geleyn, J.-F., and Banciu, D.: Cloud and
4 Precipitation Parameterization in a Meso-Gamma-Scale Operational Weather Prediction
5 Model, *Mon. Wea. Rev.*, 137, 3960-3977, 10.1175/2009mwr2750.1, 2009.

6 Ghan, S. J., and Easter, R. C.: Impact of cloud-borne aerosol representation on aerosol
7 direct and indirect effects, *Atmos. Chem. Phys.*, 6, 4163-4174, 10.5194/acp-6-4163-2006,
8 2006.

9 Grell, G., Freitas, S. R., Stuefer, M., and Fast, J.: Inclusion of biomass burning in WRF-
10 Chem: impact of wildfires on weather forecasts, *Atmos. Chem. Phys.*, 11, 5289-5303,
11 10.5194/acp-11-5289-2011, 2011.

12 Grell, G. A.: Prognostic Evaluation of Assumptions Used by Cumulus Parameterizations,
13 *Mon. Wea. Rev.*, 121, 764-787, 10.1175/1520-0493(1993)121<0764:peoaub>2.0.co;2,
14 1993.

15 Grell, G. A., and Dévényi, D.: A generalized approach to parameterizing convection
16 combining ensemble and data assimilation techniques, *Geophys. Res. Lett.*, 29, 38-31-38-
17 34, 10.1029/2002gl015311, 2002.

18 Grell, G. A., Peckham, S. E., Schmitz, R., McKeen, S. A., Frost, G., Skamarock, W. C.,
19 and Eder, B.: Fully coupled "online" chemistry within the WRF model, *Atmos. Environ.*,
20 39, 6957-6975, 10.1016/j.atmosenv.2005.04.027, 2005.

21 Grell, G. A., and Freitas, S. R.: A scale and aerosol aware stochastic convective
22 parameterization for weather and air quality modeling, *Atmos. Chem. Phys. Discuss.*, 13,
23 23845-23893, 10.5194/acpd-13-23845-2013, 2013.

24 Grell, G. A., and Freitas, S. R.: A scale and aerosol aware stochastic convective
25 parameterization for weather and air quality modeling, *Atmos. Chem. Phys.*, 14, 5233-
26 5250, 10.5194/acp-14-5233-2014, 2014.

27 Guenther, A., Karl, T., Harley, P., Wiedinmyer, C., Palmer, P. I., and Geron, C.:
28 Estimates of global terrestrial isoprene emissions using MEGAN (Model of Emissions of
29 Gases and Aerosols from Nature), *Atmos. Chem. Phys.*, 6, 3181-3210, 10.5194/acp-6-
30 3181-2006, 2006.

31 Gustafson, W. I., Qian, Y., and Fast, J. D.: Downscaling aerosols and the impact of
32 neglected subgrid processes on direct aerosol radiative forcing for a representative global
33 climate model grid spacing, *J. Geophys. Res.*, 116, D13303, 10.1029/2010jd015480,
34 2011.

35 Gustafson, W. I., Ma, P.-L., Xiao, H., Singh, B., Rasch, P. J., and Fast, J. D.: The
36 Separate Physics and Dynamics Experiment (SPADE) framework for determining

- 1 resolution awareness: A case study of microphysics, *J. Geophys. Res.*, 118, 9258-9276,
2 10.1002/jgrd.50711, 2013.
- 3 Gustafson, W. I., Jr., Chapman, E. G., Ghan, S. J., Easter, R. C., and Fast, J. D.: Impact
4 on modeled cloud characteristics due to simplified treatment of uniform cloud
5 condensation nuclei during NEAQS 2004, *Geophys. Res. Lett.*, 34, L19809,
6 10.1029/2007gl030021, 2007.
- 7 Hair, J. W., Hostetler, C. A., Cook, A. L., Harper, D. B., Ferrare, R. A., Mack, T. L.,
8 Welch, W., Izquierdo, L. R., and Hovis, F. E.: Airborne High Spectral Resolution Lidar
9 for profiling aerosol optical properties, *Appl. Opt.*, 47, 6734-6752, 2008.
- 10 Herwehe, J. A., Alapaty, K., Spero, T. L., and Nolte, C. G.: Increasing the credibility of
11 regional climate simulations by introducing subgrid-scale cloud-radiation interactions, *J.*
12 *Geophys. Res.*, 119, 2014JD021504, 10.1002/2014jd021504, 2014.
- 13 Hodzic, A., Jimenez, J. L., Madronich, S., Canagaratna, M. R., DeCarlo, P. F., Kleinman,
14 L., and Fast, J.: Modeling organic aerosols in a megacity: potential contribution of semi-
15 volatile and intermediate volatility primary organic compounds to secondary organic
16 aerosol formation, *Atmos. Chem. Phys.*, 10, 5491-5514, 10.5194/acp-10-5491-2010,
17 2010.
- 18 Hsu, Y., Strait, R., Roe, S., and Holoman, D.: SPECIATE 4.0: Speciation Database
19 Development Documentation 2006.
- 20 Janjić, Z. I.: The Step-Mountain Coordinate: Physical Package, *Mon. Wea. Rev.*, 118,
21 1429-1443, 10.1175/1520-0493(1990)118<1429:tsmcpp>2.0.co;2, 1990.
- 22 Janjić, Z. I.: Nonsingular Implementation of the Mellor-Yamada Level 2.5 Scheme in the
23 NCEP Meso model, 61, 2002.
- 24 Kain, J. S., and Fritsch, J. M.: A One-Dimensional Entraining/Detraining Plume Model
25 and Its Application in Convective Parameterization, *J. Atmos. Sci.*, 47, 2784-2802,
26 10.1175/1520-0469(1990)047<2784:aodepm>2.0.co;2, 1990.
- 27 Kain, J. S.: The Kain-Fritsch Convective Parameterization: An Update, *J. Applied*
28 *Meteor.*, 43, 170-181, 10.1175/1520-0450(2004)043<0170:tkcpau>2.0.co;2, 2004.
- 29 Koch, D., Park, J., and Del Genio, A.: Clouds and sulfate are anticorrelated: A new
30 diagnostic for global sulfur models, *J. Geophys. Res.*, 108, 4781, 10.1029/2003jd003621,
31 2003.
- 32 Larson, V. E., Schanen, D. P., Wang, M. H., Ovchinnikov, M., and Ghan, S.: PDF
33 Parameterization of Boundary Layer Clouds in Models with Horizontal Grid Spacings
34 from 2 to 16 km, *Mon. Wea. Rev.*, 140, 285-306, 10.1175/mwr-d-10-05059.1, 2012.
- 35 Lim, K.-S. S., Fan, J., Ruby Leung, L., Ma, P.-L., Singh, B., Zhao, C., Zhang, Y., Zhang,
36 G., and Song, X.: Investigation of aerosol indirect effects using a cumulus microphysics

1 parameterization in a regional climate model, *J. Geophys. Res.*, 2013JD020958,
2 10.1002/2013jd020958, 2013.

3 Ma, P. L., Rasch, P. J., Fast, J. D., Easter, R. C., Gustafson Jr, W. I., Liu, X., Ghan, S. J.,
4 and Singh, B.: Assessing the CAM5 physics suite in the WRF-Chem model:
5 implementation, evaluation, and resolution sensitivity, *Geosci. Model Dev. Discuss.*, 6,
6 6157-6218, 10.5194/gmdd-6-6157-2013, 2013.

7 Matsui, H., Koike, M., Kondo, Y., Moteki, N., Fast, J. D., and Zaveri, R. A.:
8 Development and validation of a black carbon mixing state resolved three-dimensional
9 model: Aging processes and radiative impact, *J. Geophys. Res.*, 118, 2304-2326,
10 10.1029/2012jd018446, 2013.

11 McKeen, S., Chung, S. H., Wilczak, J., Grell, G., Djalalova, I., Peckham, S., Gong, W.,
12 Bouchet, V., Moffet, R., Tang, Y., Carmichael, G. R., Mathur, R., and Yu, S.: Evaluation
13 of several PM_{2.5} forecast models using data collected during the ICARTT/NEAQS 2004
14 field study, *J. Geophys. Res.*, 112, D10S20, 10.1029/2006jd007608, 2007.

15 Morrison, H., Curry, J. A., and Khvorostyanov, V. I.: A New Double-Moment
16 Microphysics Parameterization for Application in Cloud and Climate Models. Part I:
17 Description, *J. Atmos. Sci.*, 62, 1665-1677, 10.1175/jas3446.1, 2005.

18 Morrison, H., Thompson, G., and Tatarskii, V.: Impact of Cloud Microphysics on the
19 Development of Trailing Stratiform Precipitation in a Simulated Squall Line: Comparison
20 of One- and Two-Moment Schemes, *Mon. Wea. Rev.*, 137, 991-1007,
21 10.1175/2008mwr2556.1, 2009.

22 Neale, R. B., Chen, C.-C., Gettelman, A., Lauritzen, P. H., Park, S., Williamson, D. L.,
23 Conley, A. J., Garcia, R., Kinnison, D., Lamarque, J. F., Marsh, D., Mills, M., Smith, A.
24 K., Tilmes, S., Vitt, F., Morrison, H., Cameron-Smith, P., Collins, W. D., Iacono, M. J.,
25 Easter, R. C., Ghan, S. J., Liu, X., Rasch, P. J., and Taylor, M. A.: Description of the
26 NCAR Community Atmosphere Model (CAM 5.0), NCAR, 2012.

27 Ntelekos, A. A., Smith, J. A., Donner, L., Fast, J. D., Gustafson, W. I., Chapman, E. G.,
28 and Krajewski, W. F.: The effects of aerosols on intense convective precipitation in the
29 northeastern United States, *Quarterly Journal of the Royal Meteorological Society*, 135,
30 1367-1391, 10.1002/qj.476, 2009.

31 Pfister, G. G., Avise, J., Wiedinmyer, C., Edwards, D. P., Emmons, L. K., Diskin, G. D.,
32 Podolske, J., and Wisthaler, A.: CO source contribution analysis for California during
33 ARCTAS-CARB, *Atmos. Chem. Phys.*, 11, 7515-7532, 10.5194/acp-11-7515-2011,
34 2011.

35 Qian, Y., Gong, D., Fan, J., Leung, L. R., Bennartz, R., Chen, D., and Wang, W.: Heavy
36 pollution suppresses light rain in China: Observations and modeling, *J. Geophys. Res.*,
37 114, n/a-n/a, 10.1029/2008jd011575, 2009.

- 1 Shrivastava, M., Lane, T. E., Donahue, N. M., Pandis, S. N., and Robinson, A. L.: Effects
2 of gas particle partitioning and aging of primary emissions on urban and regional organic
3 aerosol concentrations, *J. Geophys. Res.*, 113, n/a-n/a, 10.1029/2007jd009735, 2008.
- 4 Shrivastava, M., Fast, J., Easter, R., Gustafson Jr, W. I., Zaveri, R. A., Jimenez, J. L.,
5 Saide, P., and Hodzic, A.: Modeling organic aerosols in a megacity: comparison of
6 simple and complex representations of the volatility basis set approach, *Atmos. Chem.*
7 *Phys.*, 11, 6639-6662, 10.5194/acp-11-6639-2011, 2011.
- 8 Shrivastava, M., Berg, L. K., Fast, J. D., Easter, R. C., Laskin, A., Chapman, E. G.,
9 Gustafson, W. I., Liu, Y., and Berkowitz, C. M.: Modeling aerosols and their interactions
10 with shallow cumuli during the 2007 CHAPS field study, *J. Geophys. Res.*, 1343-1360,
11 10.1029/2012jd018218, 2013.
- 12 Skamarock, W. C., Klemp, J. B., Dudhia, J., Gill, D. O., Barker, D. M., Duda, M. G.,
13 Huang, X.-Y., Wang, W., and Powers, J. G.: A Description of the Advanced Research
14 WRF Version 3, NCARNCAR/TN-475+STR, 2008.
- 15 Solomon, S., Qin, D., Manning, M., Alley, R. B., Berntsen, T., Bindoff, N. L., Chen, Z.,
16 Chidthaisong, A., Gregory, J. M., Hegerl, G. C., Heimann, M., Hewitson, B., Hoskins, B.
17 J., Joos, F., Jouzel, J., Kattsov, V., Lohmann, U., Matsuno, T., Molina, M., Nicholls, N.,
18 Overpeck, J., Raga, G., Ramaswamy, V., Ren, J., Rusticucci, M., Somerville, R., Stocker,
19 T. F., Whetton, P., Wood, R. A., and Wratt, D.: Technical Summary., in: *Climate Change*
20 *2007: The Physical Science Basis. Contribution of Working Group I to the Fourth*
21 *Assessment Report of the Intergovernmental Panel on Climate Change*, edited by:
22 Solomon, S., Qin, D., Manning, M., Chen, Z., Marquis, M., Averyt, K. B., Tignor, M.,
23 and Miller, H. L., Cambridge University Press, Cambridge, United Kingdom and New
24 York, NY, USA, 2007.
- 25 Stevens, B., and Feingold, G.: Untangling aerosol effects on clouds and precipitation in a
26 buffered system, *Nature*, 461, 607-613, 2009.
- 27 Stull, R. B.: A fair-weather cumulus cloud classification scheme for mixed-layer studies,
28 *J. Climate Appl. Meteor.*, 24, 49-56, 1985.
- 29 Tsimpidi, A. P., Karydis, V. A., Zavala, M., Lei, W., Molina, L., Ulbrich, I. M., Jimenez,
30 J. L., and Pandis, S. N.: Evaluation of the volatility basis-set approach for the simulation
31 of organic aerosol formation in the Mexico City metropolitan area, *Atmos. Chem. Phys.*,
32 10, 525-546, 10.5194/acp-10-525-2010, 2010.
- 33 Wang, H., Rasch, P. J., and Feingold, G.: Manipulating marine stratocumulus cloud
34 amount and albedo: a process-modelling study of aerosol-cloud-precipitation interactions
35 in response to injection of cloud condensation nuclei, *Atmos. Chem. Phys.*, 11, 4237-
36 4249, 10.5194/acp-11-4237-2011, 2011.
- 37 Wang, H., Easter, R. C., Rasch, P. J., Wang, M., Liu, X., Ghan, S. J., Qian, Y., Yoon, J.
38 H., Ma, P. L., and Vinoj, V.: Sensitivity of remote aerosol distributions to representation

1 of cloud–aerosol interactions in a global climate model, *Geosci. Model Dev.*, 6, 765-782,
2 10.5194/gmd-6-765-2013, 2013.

3 Wiedinmyer, C., Akagi, S. K., Yokelson, R. J., Emmons, L. K., Al-Saadi, J. A., Orlando,
4 J. J., and Soja, A. J.: The Fire INventory from NCAR (FINN): a high resolution global
5 model to estimate the emissions from open burning, *Geosci. Model Dev.*, 4, 625-641,
6 10.5194/gmd-4-625-2011, 2011.

7 Wyngaard, J. C.: Toward Numerical Modeling in the “Terra Incognita”, *J. Atmos. Sci.*,
8 61, 1816-1826, 10.1175/1520-0469(2004)061<1816:tnmitt>2.0.co;2, 2004.

9 Zaveri, R. A., Easter, R. C., Fast, J. D., and Peters, L. K.: Model for Simulating Aerosol
10 Interactions and Chemistry (MOSAIC), *J. Geophys. Res.*, 113, D13204,
11 10.1029/2007jd008782, 2008.

12 Zhang, G. J., and McFarlane, N. A.: Sensitivity of climate simulations to the
13 parameterization of cumulus convection in the Canadian climate centre general
14 circulation model, *Atmosphere-Ocean*, 33, 407-446, 10.1080/07055900.1995.9649539,
15 1995.

16 Zhao, C., Liu, X., Ruby Leung, L., and Hagos, S.: Radiative impact of mineral dust on
17 monsoon precipitation variability over West Africa, *Atmos. Chem. Phys.*, 11, 1879-1893,
18 10.5194/acp-11-1879-2011, 2011.

19 Zhao, C., Chen, S., Leung, L. R., Qian, Y., Kok, J. F., Zaveri, R. A., and Huang, J.:
20 Uncertainty in modeling dust mass balance and radiative forcing from size
21 parameterization, *Atmos. Chem. Phys.*, 13, 10733-10753, 10.5194/acp-13-10733-2013,
22 2013.

23
24
25

1 Table 1. WRF-Chem configuration used in this study

Physical Process	Parameterization
Surface	Noah land-surface model (Chen et al., 1996)
Boundary layer	Mellor-Yamada-Janjić (Janjić, 1990, 2002)
Cloud microphysics	Morrison two moment (Morrison et al., 2005; Morrison et al., 2009)
Cumulus	Kain-Frisch (with CuP modifications) (Kain and Fritsch, 1990; Kain, 2004; Berg et al., 2013)
Radiation (shortwave and longwave)	CAM 3 (Collins et al., 2004)
Gas-phase chemistry	SAPRC-99 (Carter, 2010)
Aerosol chemistry	MOSAIC for inorganic aerosols (Zaveri et al., 2008); Simplified Volatility Basis Set (VBS) for organic aerosol (Shrivastava et al., 2011)

2

3

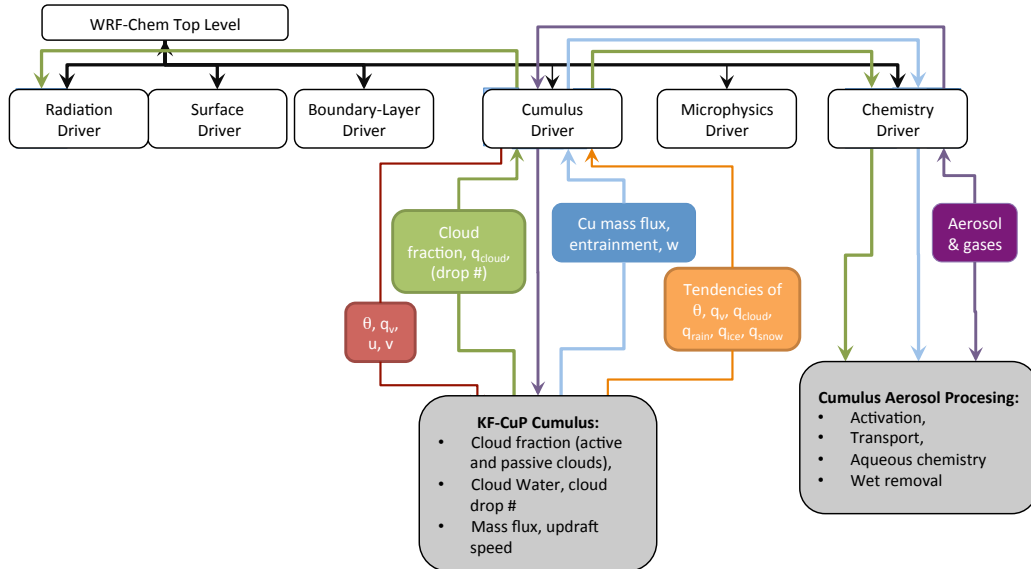
1 Table 2. Definitions of simulations completed as part of the study. The parameterized
2 cumulus dynamics are applied in all simulations.

Simulation	Aerosol Processing by Shallow and Deep Cu
DeepShallow	Aerosol Processing Shallow Cu: On Aerosol Processing Deep Cu: On
ShallowOnly	Aerosol Processing Shallow Cu: On Aerosol Processing Deep Cu: Off
Control	Aerosol Processing Shallow Cu: Off Aerosol Processing Deep Cu: Off

3

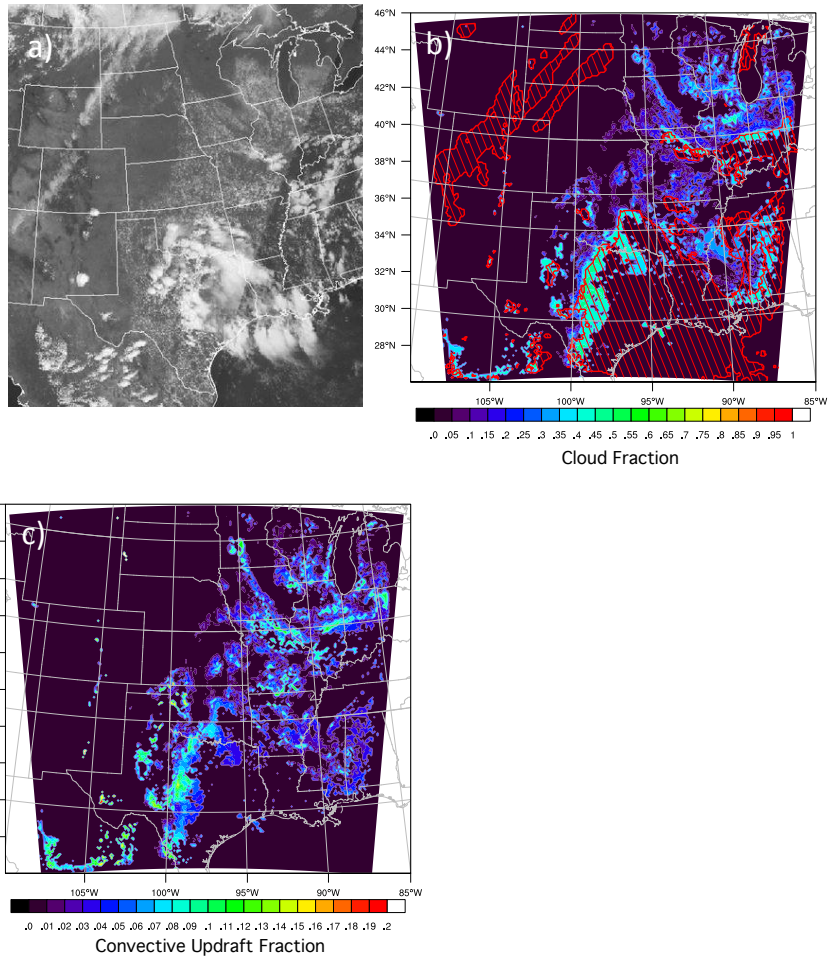
4

1 Figures

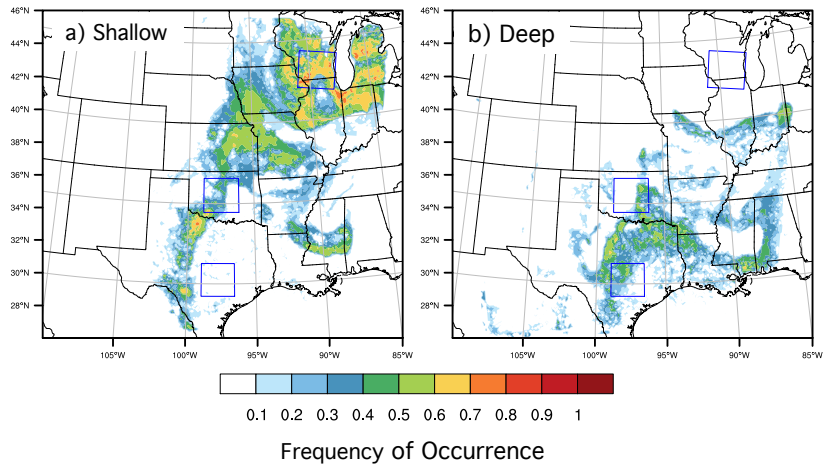


2

3 Figure 1. Summary of modifications to the standard implementation of WRF-Chem.
 4 Colored boxes indicate information passed between subroutines related to the
 5 thermodynamics (red), cloud microphysical and macrophysical properties (green), cloud
 6 dynamics (blue), thermodynamic tendencies (orange) and aerosol and trace gases
 7 (purple), while gray boxes indicate the new or modified parameterizations applied in
 8 WRF-Chem. Arrows indicate information flow within the model. Note that the droplet
 9 number generated in the KF-CuP parameterization is not currently used in the Radiation
 10 Driver.

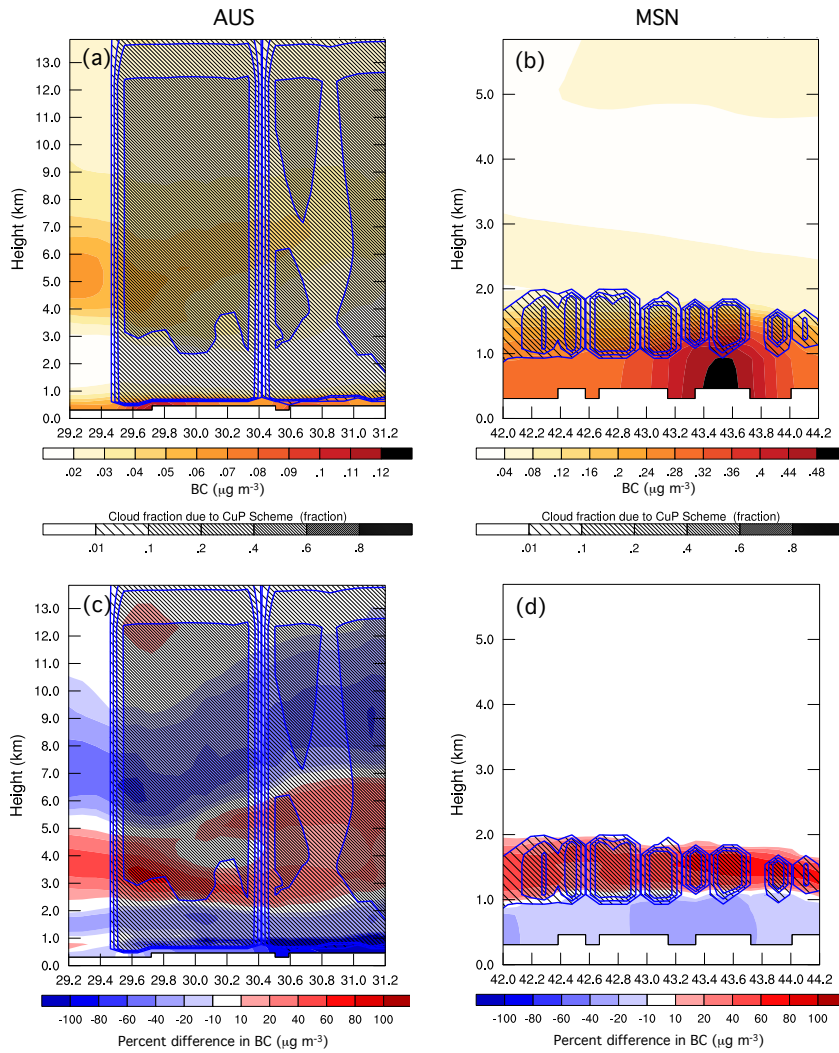


1
 2 Figure 2. GOES visible satellite image valid at 20:15 UTC, 25 June 2007 (a), and
 3 simulated cloud fraction associated with the KF-CuP parameterization (colors), areas
 4 with grid resolved clouds (hashed; b), and fraction of model grid box with convective
 5 updrafts (c). Note different color scales used in plots of cloud fraction (b) and convective
 6 updraft fraction (c).



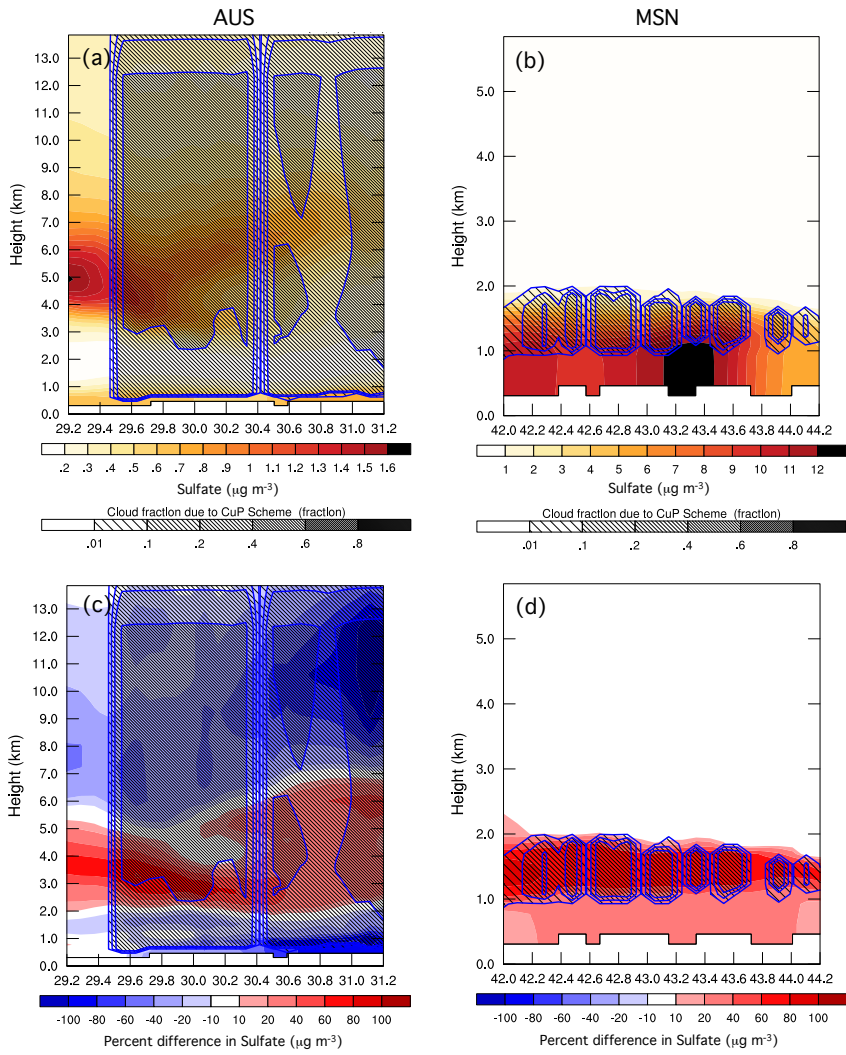
1

2 Figure 3. Frequency of occurrence of deep convection (right) and shallow convection
3 (left) for the time period 12:00-20:00 UTC on 25 June, 2007. Boxes indicate sub regions,
4 240 km on a side, selected for analysis.



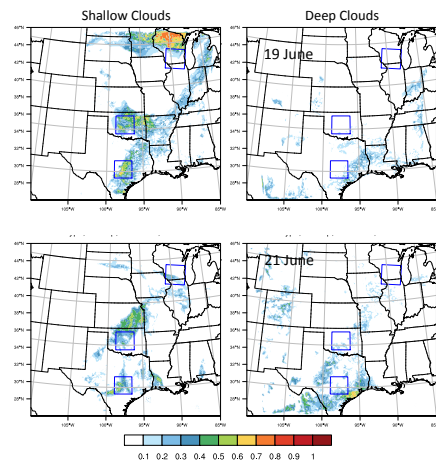
1

2 Figure 4. Vertical north-south cross sections of BC in size bins 1 through 4 (colors top;
 3 $\mu\text{g kg}^{-1}$), including both interstitial and activated aerosol in the cloudy grid cells, and
 4 difference in BC mass loading between DeepShallow and control simulations (colors
 5 bottom; percentage) for conditions dominated by deep convective clouds (AUS; left) and
 6 shallow convective clouds (MSN; right) boxes at 20 UTC on 25 June, 2007. Hatching
 7 indicates cloud fraction associated with sub-grid convective clouds. The horizontal axis is
 8 labeled in degrees of latitude and heights are height above mean sea level.



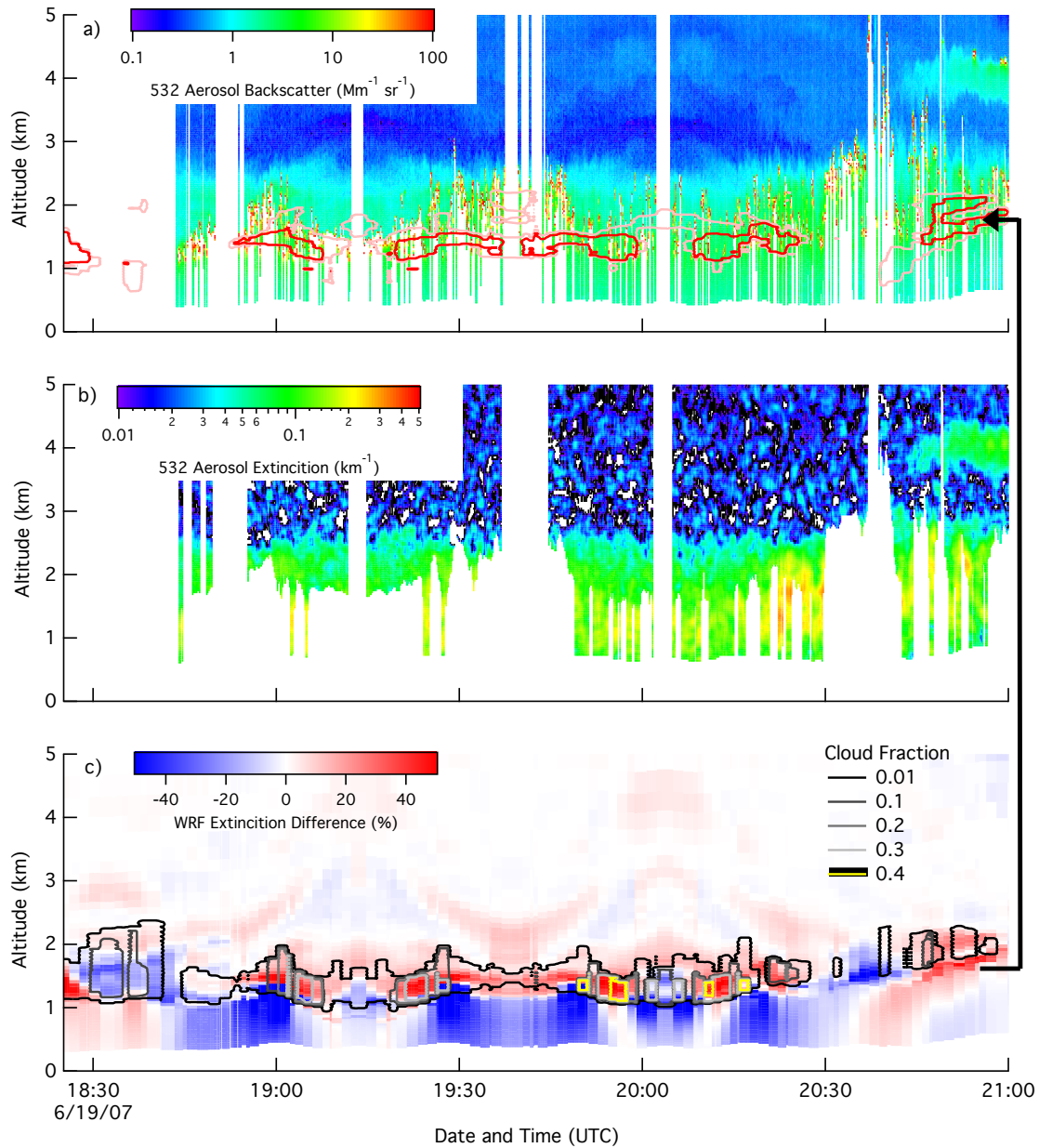
1

2 Figure 5. Same as Figure, but for sulfate.

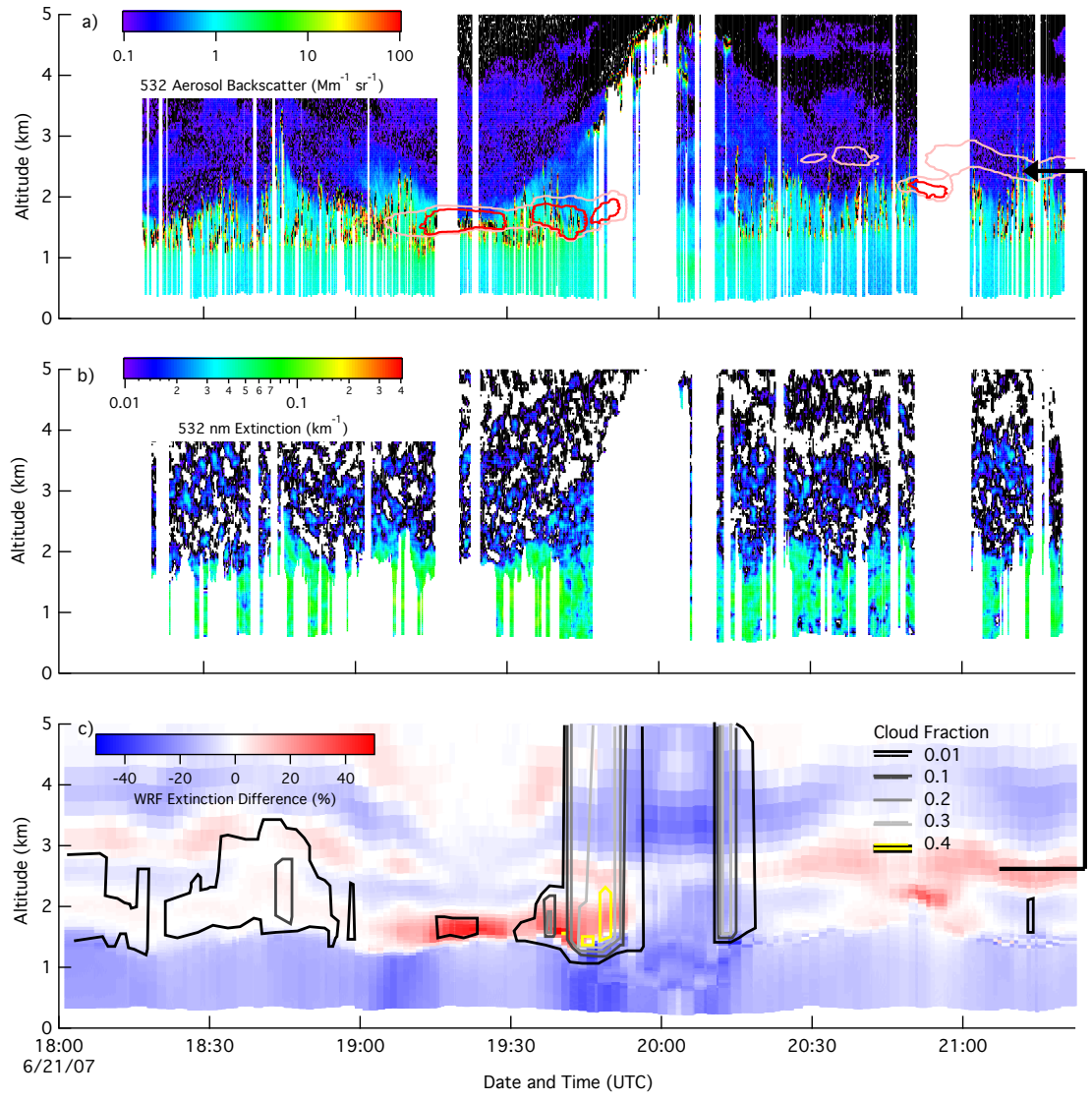


1

2 Figure 6. Frequency of occurrence of deep convection (right) and shallow convection
 3 (left) for the time period 12:00-20:00 UTC on 19 (top) and 21 June (bottom), 2007.



1
 2 Figure 7. Cross sections of observed aerosol backscatter (top), aerosol extinction (middle)
 3 at a wavelength of 532 nm, and difference in aerosol extinction of DeepShallow and
 4 Control simulations (bottom) on 19 June 2007. Contours in (a) mark contours of +10 and
 5 +20% difference in the WRF-Chem simulations, as indicated by the large arrow, and
 6 contours in (c) indicate simulated cloud fraction as indicated by the legend.

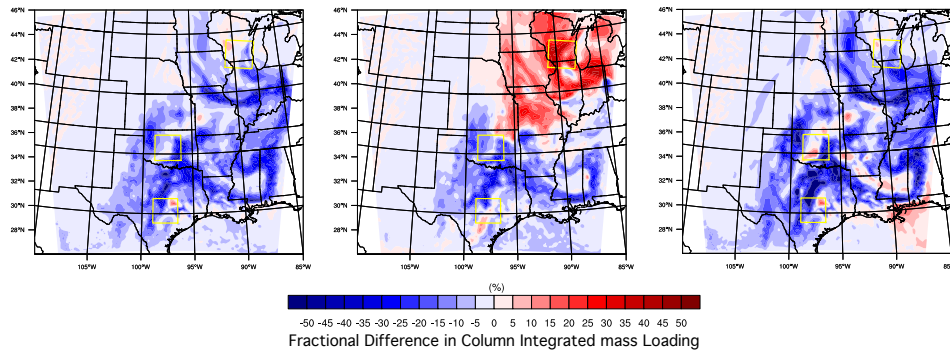


1

2 Figure 8. Same as Figure 7 but for 21 June 2007.

3

1



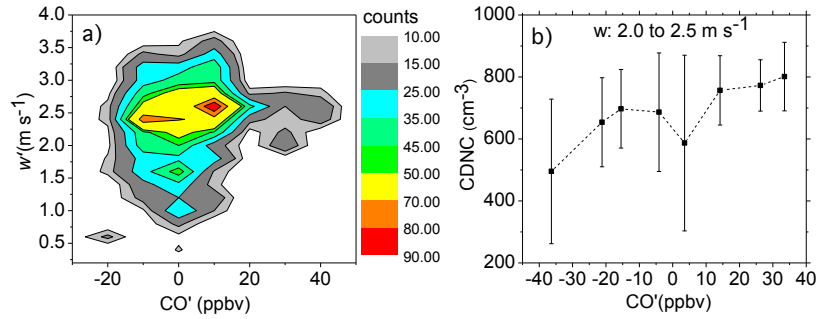
2

3

4 Figure 9. Fractional differences in column integrated aerosol mass loading between
5 DeepShallow and control simulations for size bins 1 through 4, including both interstitial
6 and activated aerosol in the cloudy grid cells, for BC (left), sulfate (center) and OA
7 (right), valid at 20:00 UTC on 25 June, 2007. Yellow boxes indicate boxes used in the
8 analysis.

9

1

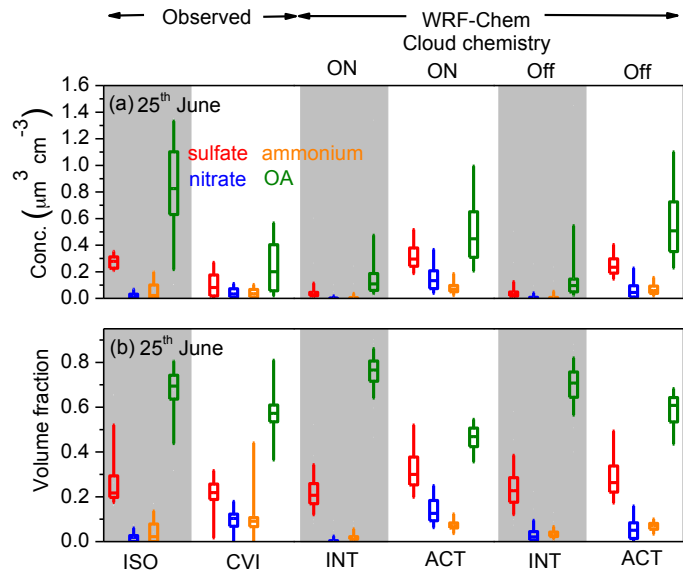


2

3 Figure 10. PDF of simulated cloud updraft speed and CO loading in cloudy updrafts (a),
4 change in CDNC with perturbation values of CO (CO') for perturbation values of w' (w')
5 between 2.0 and 2.5 m s^{-1} (b). Error bars in (b) indicate the standard deviation.

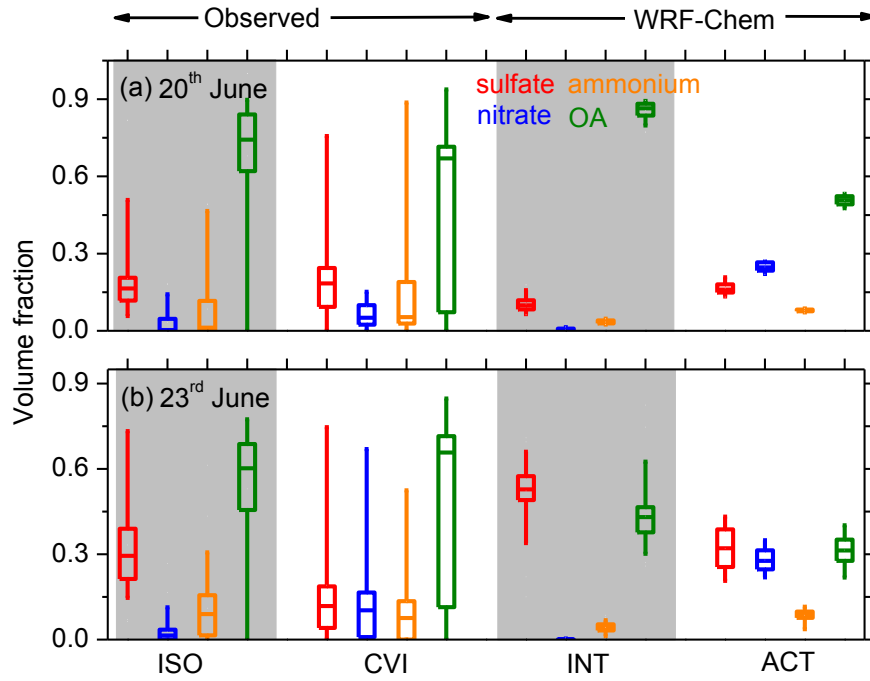
6

1



2

3 Figure 11. Aerosol mass concentration (top) and volume fraction (bottom) for observed
4 interstitial [sampled via an isokinetic inlet (ISO; grey areas)] and activated [sampled via a
5 counter-flow virtual impactor inlet (CVI; white areas)] aerosol; and simulated interstitial
6 (INT; grey areas) and activated (ACT; white areas) aerosol at 20:00 UTC on 25 July,
7 2007. Colors indicate sulfate (red), ammonium (orange), nitrate (blue), and organic
8 aerosol (green) in size bins 1 through 4. Box-and-whisker plots indicate 90th, 75th, 50th,
9 25th, and 10th percentiles.



1

2

3 Figure 12. Similar to Figure 11, but for only aerosol volume fraction on 20 and 23 June
 4 2007. WRF-Chem results are only for cases in which the aqueous chemistry is turned on.

5